5-5-2014

Nitrogen Isotope Dynamics of Anammox and Denitrification in Coastal Groundwater

Nicole Chang
University of Connecticut - Avery Point, nicole.chang@uconn.edu

Nitrogen Isotope Dynamics of Anammox and Denitrification in Coastal Groundwater

Nicole Whi-tzen Chang

B.A., Duke University, 2010

A Thesis

Submitted in Partial Fulfillment of the

Requirements for the Degree of

Master of Science

at the

University of Connecticut

2014

APPROVAL PAGE

Master of the Science Thesis

Nitrogen Isotope Dynamics of Anammox and Denitrification in Coastal Groundwater

Presented by

Nicole Whi-tzen Chang, B.A.

Major Advisor _____
Craig R. Tobias

Associate Advisor _____
Julie Granger

Associate Advisor _____
Penny Vlahos

University of Connecticut

2014

ACKNOWLEDGEMENTS

I would like to express my deepest appreciation and gratitude to my advisor Dr. Craig Tobias, without whom I could not have attained this achievement. Thank you for all the knowledge, aid, advice, editing, and patience you have given for the past two and a half years. I would also like to thank my committee members, Dr. Penny Vlahos and Dr. Julie Granger, for their help and occasional usage of their labs. Thank you to our colleagues at the U.S. Geological Survey, through field work, snow, shotgun hunting season, and government shutdowns, for both analytical work and use of facilities and equipment during the countless trips to the Cape. Finally, thank you to Dave Cady and Claudia Koerting for all of their help during lab analyses, Kevin Brown for modeling, those of the night crew, and all my family, friends, and fellow labmates for their support.

TABLE OF CONTENTS

LIST OF TABLES vi

LIST OF FIGURES vii

ABSTRACT viii

INTRODUCTION 10

MATERIALS AND METHODS 17

Study Site 17

Experimental Approach 21

Natural Abundance Incubations 21

Tracer Incubations 22

Analytical Methods 23

Data Synthesis 24

Natural Abundance 24

Tracer 27

RESULTS 28

Natural Abundance Fractionation Experiments 28

Upgradient F575 Site 28

Downgradient F168 Site 33

Rayleigh-derived Apparent Isotope Enrichment Factors 40

^{15}N Tracer Incubation Experiment – F168 46

DISCUSSION 49

Co-occurrence of Denitrification and Anammox 49

Organic Carbon Induced Shift to Denitrification 51

NO_x Isotopes as a Diagnostic of Anammox 53

Ammonium Isotopes as a Diagnostic 54

Isotope Modeling 56

Summary 64

REFERENCES 65

LIST OF TABLES

Table Page

1. Experimental treatments by year, depth, and amendment 20

2. Effective enrichment factors 45

LIST OF FIGURES

Figure Page

1. Cape Cod plume site map 18

2. Depth profiles of selected chemical gradients at upgradient and downgradient sites 19

3. F575 2011 Natural Abundance Incubations 30

4. F575 2012 Natural Abundance Incubations 33

5. F168 2012 Natural Abundance Incubations 36

6. F168 2013 Natural Abundance Incubations 39

7. $\delta^{15}(NO_{3+2})$ Rayleigh-derived Isotope Enrichment Factors 42

8. $\delta^{15}(NO_2)$ Rayleigh-derived Isotope Enrichment Factors 43

9. $\delta^{15}(NH_4^+)$ Rayleigh-derived Isotope Enrichment Factors 44

10. F168 2013 Tracer Incubations 48

11. Model Fits and Parameters for F575 2012 #MI 59

12. Model Fits and Parameters for F168 2012 #MI 60

13. Model Fits and Parameters for F575 2012 CMI 62

14. Model Fits and Parameters for F168 2012 CMI 63

ABSTRACT

The relative inaccessibility of aquifers and co-occurrence of denitrification contribute to difficulties in assessing anammox contribution to total environmental N_2 production in this system. Anaerobic ammonium oxidation (anammox) is an autotrophic microbial process that converts NO_2^- and NH_4^+ into nitrogen gas (N_2), an alternate to denitrification in the nitrogen cycle. This process may be important in attenuating fixed nitrogen in groundwater prior to discharge into coastal systems. Nitrogen isotope enrichment factors have proven useful in identifying dominant processes within the overall nitrogen cycle in various environments, but the approach has not yet been directed at anammox outside of a pure culture setting. The influence of anammox on the nitrogen isotope dynamics of DIN species and N_2 was assessed through controlled laboratory incubations using groundwater and sediment from a nitrogen-contaminated groundwater plume with characterized anammox activity. These were conducted under conditions of varied anammox contribution to total N_2 production. Experimentally observed enrichment factors associated with nitrate (NO_3^-) and nitrite (NO_2^-) reduction ranged from -17 to -25‰ regardless of treatment. A finite time stepping model modified from Böhlke (2001) and Böhlke et al. (2002) was then used to determine a set of enrichment factors for the natural abundance incubations representing "best fits" for concentrations and isotope evolution of DIN species, N_2, and N_2O concentration. The modeled isotopic effects in the NO_2^- and NO_3^- pools were on a similar scale to that of denitrification and all greater than -30‰. This finding was consistent with results from separate ^{15}N tracer experiments that suggested anammox accounts for up to 8 or 28% of N_2 production, depending on weighting of denitrification within treatments. NH_4^+ fractionations could not be clearly discerned from observed or modeled data likely because

of low rates, a large NH_4^+ pool, and isotopic exchange between aqueous and sediment NH_4^+ pools. Nitrogen isotope systematics appeared to be dominated by denitrification, and good modeled fits to experimental data could be attained within the range of published denitrification enrichment factors with or without anammox. This work highlights the challenges in interpreting *in situ* patterns of $\delta^{15}N$ as unique indicators of anammox.

INTRODUCTION

Human activities have almost doubled the rate of nitrogen input to terrestrial systems (Vitousek et al. 1997). Watershed export of fixed nitrogen by rivers and streams ultimately deposits into the nitrogen-limited coastal ocean. This region, which accounts for half of the global ocean's primary production (Paerl 1997), is disproportionally affected by the nitrogen input (Galloway et al. 2003), resulting in eutrophication, harmful algal blooms (Paerl 1997; Vitousek et al. 1997; Howarth and Marino 2006), ecological shifts towards lower trophic levels (Deegan et al. 2002), and changes in species composition (Hillebrand et al. 2000).

Increased delivery of watershed nitrogen to the continental margin can be offset by the removal of reactive N from surface and groundwater during transport. Only two known processes in the nitrogen cycle return fixed N to the form of N_2: denitrification and anaerobic ammonium oxidation (anammox; Dalsgaard et al. 2005; Seitzinger et al. 2006; reviewed by Song and Tobias 2011). Both reactions are microbially catalyzed and require anaerobic conditions.

Denitrification has been historically considered the primary mechanism of N_2 production. Denitrifying bacteria use oxidized nitrogen species (NO_x) (Seitzinger et al. 2006; Eq 1) as terminal electron acceptors during respiration. A wide diversity of bacteria can perform denitrification either obligately or facultatively (reviewed by Robertson et al. 1989; Seitzinger et al. 2006) in anoxic water columns and/or sediments. Nitrate (NO_3^-) is reduced to nitrite (NO_2^-) via the dissimilarity nitrate reductase (NaR). Nitrite reductase (cytochrome cd_1) (NiR) reduces NO_2^- to nitric oxide (NO), which is itself reduced to N_2O via nitric-oxide reductase (NOR). Finally, N_2O reductase (NOS) converts N_2O to N_2 (Körner and Zumft 1989).

Eq. 1) $OC + NO_3^- \rightarrow NO_2^- \rightarrow NO \rightarrow N_2O \rightarrow N_2\,(g)$

NaR NiR NOR NOS

Denitrification can terminate at N_2O in limited electron environments and/or under trace oxygen conditions (Seitzinger et al. 2006) which can affect total N_2O emissions in terrestrial and aquatic systems (Bouwman et al. 1995; Huang et al. 2008). In surface water and terrestrial environments, organic carbon (OC) is the ultimate electron donor for all reaction steps, while OC and mineral phase electron donors (e.g. reduced sulfate) can also support denitrification in groundwater (Böhlke and Denver 1995; Appelo and Postma 2005). The oxidized nitrogen NO_3^- and/or NO_2^- can be supplied from the aqueous phase (e.g. diffusion from the water column), or denitrification can be tightly coupled to sedimentary sources of NO_x produced locally from nitrification in adjacent oxic microzones (Risgaard-Petersen 2003, Seitzinger et al. 2006).

Anammox, which also requires an anoxic environment, uses ammonium (NH_4^+) as the source of electrons to reduce NO_2^- to N_2 (Eqs. 2, 3). Unlike denitrification, which is heterotrophic, anammox bacteria are chemolithotrophic and capable of fixing inorganic carbon with electrons afforded by ammonium (Sliekers et al. 2002). Only a few species of bacteria have been identified that are capable of performing the anammox reaction (*Candidatus Brocadia anammoxidans, Candidatus Brocadia brodae, Candidatus Scalindua wagneri, Candidatus Scalindua sorokinii, Candidatus Anammoxoglobus propionicus*) (Strous et al. 1999; Schmid et al. 2003; Dale et al. 2009; Kartal et al. 2008). NO_2^- is initially reduced to NO via nitrite reductase (NiR). The NO then reacts with ammonium (NH_4^+) through the hydrazine oxidoreductase (HZO) enzyme to form a short-lived hydrazine (N_2H_4) intermediate (Schalk et al. 1998). Breakdown of the unstable N_2H_4 forms N_2 which contains one N from NO_2^- and the other

from NH_4^+. All reactions take place within an organelle specific to annamox bacteria called the annamoxosome, where ladderane lipids make up a membrane that protects the reaction from trace amounts of O_2 (Strous et al. 2006, Dalsgaard et al. 2005**;** Kalvelage et al. 2011).

Eq. 2) $NO_2^- \rightarrow NO + NH_4^+ \rightarrow N_2H_4 \rightarrow N_2 + H_2O$

NiR HZO

Simplified, the reaction is as follows:

Eq. 3) $NH_4^+ + NO_2^- \rightarrow N_2 + 2H_2O$

For anammox, the NH_4^+ serves as the electron donor and no external source of organic carbon is required for the redox reaction, although there is evidence that anammox can use low molecular weight organic carbon substrates such as formate (Smith et al. 2001; Kartal et al. 2007), but with little significant influence on overall rate of N_2 production. Anaerobic degradation of organic matter supplies NH_4^+ in anammox amenable environments, as does anthropogenic waste disposal. The NO_2^- substrate appears in the water column as an intermediate from aerobic ammonium oxidation (e.g. nitrification; Mulder et al. 1995; Siegrist et al. 1998; Third et al. 2005; Lam et al. 2007), and/or following the nitrate reduction step of denitrification (Song and Tobias 2011; Trimmer et al. 2005; Dalsgaard et al. 2005), and/or dissimilatory nitrate reduction to ammonium (DNRA; Giblin et al. 2013). The common NO_2^- substrate shared between anammox, denitrification, and nitrification, as well as potentially NH_4^+ between anammox and DNRA, provide challenges to studying anammox *in situ*.

Denitrification has been exhaustively measured in terrestrial soils (Seitzinger et al. 2006), groundwater (Mariotti et al. 1988; Smith et al. 1991, 2001; Schmidt et al. 2011), wetlands (Seitzinger et al. 2006; Burgin et al. 2010; Harrison et al. 2011), and coastal zones (An and Joye 2001; Risgaard-Petersen 2003). Anammox measurements in surface water environments have similarly been carried out with increasing frequency since the reaction's discovery (Dalsgaard et al. 2005; Hamersley et al. 2009). N_2 production previously attributed solely to denitrification has proven to be a mixture of N_2 produced by both processes (Risgaard-Petersen et al. 2003) in various settings. Anammox has been identified in locations such as anoxic water columns of the Black Sea (Kuypers et al. 2003; Lam et al. 2007) and Golfo Dulce (Dalsgaard et al. 2003), Arctic sea ice (Rysgaard and Glud 2004), coastal sediments such as those of the Thames estuary (Trimmer et al. 2003), lake sediments (Souza et al. 2012), and oxygen minimum zones of the ocean water column (Thamdrup et al. 2006). Except for a handful of studies in contaminated aquifers (Clark et al. 2008, Moore et al. 2011; Robertson et al. 2012), quantification of groundwater anammox has largely escaped attention.

Groundwater acts as a long term repository for terrestrial nitrogen and represents both a significant water resource and a delivery route for nitrogen loads that ultimately deposit in the coastal ocean, either directly or by discharge to streams and rivers (Giblin and Gaines 1990; Lyngkilde and Christensen 1992; Valiela et al. 1997, 1999; Cole et al. 2006; Swartz et al. 2006; Robertson et al. 2012). While aquifers vary widely in redox state and speciation of dissolved nitrogen concentration, much of the organic carbon is typically respired soon after recharge and thus tends to be organic-carbon poor relative to their surface water counterparts. Those aquifers that are N-rich, anaerobic, and carbon poor should be favorable for anammox (Clark et al. 2008).

Recent global estimates of in-aquifer conversion of reactive N to N_2 are based on organic carbon proxies for denitrification. Because these estimates (20% of global N_2 production from denitrification in freshwater) were derived using organic carbon as a proxy (Bouwman et al. 2002; Seitzinger et al. 2006) and anammox does not require an external source of OC, it is conceivable that current groundwater global N_2 production values are underestimating the contribution of anammox.

Biogeochemical reactions in general, and anammox and denitrification in particular, are difficult to study in aquifers due to relative inaccessibility of reaction sites. Molecular approaches have been useful for identifying genes of free living bacteria in groundwater, but these measurements do not necessarily correlate with activity, and Quantitative PCR (qPCR) approaches for anammox gene expression are only now maturing (Song and Tobias 2011) and have yet to be calibrated as proxies for rates. In order to derive these reaction rates, hydrogeologists and geochemists have approached this problem by examining changes in chemical ratios (e.g. N_2/Ar) along flow paths, and also by turning to *in situ* tracer experiments coupled to advection-dispersion models to derive reaction rates (Garabedian et al. 1991; Tobias et al. 2001; Smith et al. 2004; Böhlke et al. 2006; Roberston et al. 2012; Jahangir et al. 2013). One such approach used to identify numerous different nitrogen cycle reactions, including denitrification in aquifers *in situ*, is natural abundance ^{15}N stable isotopes ($\delta^{15}N$).

All natural abundance isotopic values are expressed in the delta notation ($\delta^{15}N$) in units of per mille according to:

Eq. 4) $$\delta = [(R_{sample}/R_{standard}) - 1] \times 1000‰$$

Where R is the ratio of the heavy to the light isotope, and the nitrogen standard is set at 0‰ for atmospheric nitrogen.

The distribution of stable isotope ratios has been used previously in other groundwater studies involving denitrification (Mariotti et al. 1982, 1988; Böhlke et al. 2004, 2009; Green et al. 2010), and has more recently been applied to infer anammox activities in aquifers. For example, Clark et al. (2008) examined an aquifer with a history of ammonium contamination from nearby chemical and fertilizer companies. Using well surveys across the downstream flowpath and mixing curves, the study concluded that that the enrichment of $\delta^{15}NO_3$ and $\delta^{15}NH_4^+$ indicated a reactive loss of both substrates. Combined with an overpressuring N_2 gas increase, anammox was suggested as the mechanism of N loss. Similarly, during an *in situ* experiment, Robertson et al. (2011) found enrichment in $\delta^{15}NH_4^+$ over a gradient at a site abundant in anammox bacteria, correspondent with $NH4^+$ attenuation, suggesting anammox as a possible active process. In a laboratory incubation experiment using two sites with anammox bacteria present, Moore et al. (2011) found up to 18 and 36% of groundwater N_2 production attributable to anammox. Studies such as these show the usefulness of stable isotope distributions in inferring the contribution of individual reactions to the extant N pools. However, these groundwater anammox studies only represent a start. A more robust use of natural abundance N isotopes to assess the relative prevalence of anammox in aquifers where denitrification may also be present requires a refined understanding of how each of these reactions fractionate the various DIN species in each of the reaction pathways. Many of these fractionation factors (α) have been studied for steps in denitrification pathways in cultures (Granger et al. 2008; Kritee et al. 2012) and in the environment (Mariotti et al. 1981; Voss et al. 2001; Böhlke et al. 2006, Perez et al. 2006; Sutka et al. 2008;). The lack of widely available pure anammox cultures has until recently

hampered estimation of anammox fractionation factors in culture (Brunner et al. 2013), though there are estimates from the environment based on localized ^{15}N enrichment of ammonium in anaerobic marine sediments (Prokopenko et al. 2013).

The fractionation factor (α) describes the relative difference in the reaction rates of heavy and light isotopologues during a unidirectional reaction, and here is defined by the ratio of the rate constants (k) for a reaction regarding ^{15}N and ^{14}N (Mariotti et al. 1981) (Eq 5).

Eq. 5) $\alpha = {}^{15}kN/{}^{14}kN$

Eq. 6) $\varepsilon = (\alpha - 1) \times 1000$

The term α is often reported as the enrichment factor (epsilon, ε), reported in per mille (‰) units; Eq 6, the proportion by which the product of the reaction is enriched by the heavier isotope in relation to the substrate (Mariotti et al. 1981).

Here we describe a series of experiments designed to establish enrichment factors associated with the production and/or consumption of the DIN species participating in the anammox reaction, as manifested in a nitrogen contaminated shallow coastal aquifer. Anammox activity has been detected at this aquifer, co-occuring with variable amounts of denitrification. The overarching objective of this study was to determine whether specific N isotope fractionations are unique to anammox, and can serve as a diagnostic for anammox when applied to broader aquifer-scale surveys of $\delta^{15}N$-DIN.

MATERIALS AND METHODS

STUDY SITE

A series of natural abundance isotope fractionation incubation experiments and a single ^{15}N tracer experiment were conducted using aquifer sediments collected from a nitrogen contaminated wastewater groundwater plume located on Cape Cod, MA (Figure 1). Though the sewage disposal via infiltration beds was discontinued in 1995, the legacy plume still exists at dimensions of 6 km long, 1 km in width, and 23 m in thickness. Two locations in the plume – upper and lower plume – were chosen for the study. The upper plume location (F575; 41°38'11.74"N, 70°32'31.52"W) is located 300 m from the infiltration beds. The lower plume location (F168; 41°37'1.64"N, 70°32'56.24"W) is located 2 km downgradient in the Ashumet Valley (USGS Cape Cod Toxics 2013). These two locations were chosen as sites sufficiently suboxic to support anammox, and whose potential activity was confirmed by ^{15}N tracer and the presence of the HZO functional gene (Song et al. 2010). Denitrification has been reported at both sites, with higher rates at F575 closer to the infiltration beds, and lower rates at F168 where denitrification is thought to be limited by the availability of labile DOC (Thurman et al. 1986; Smith and Duff 1988; Smith et al. 1991; Barbaro et al. 2013**)**. Aquifer sediments and groundwater were collected From F575 in 2011 and 2012, and from F168 in 2012 and 2013.

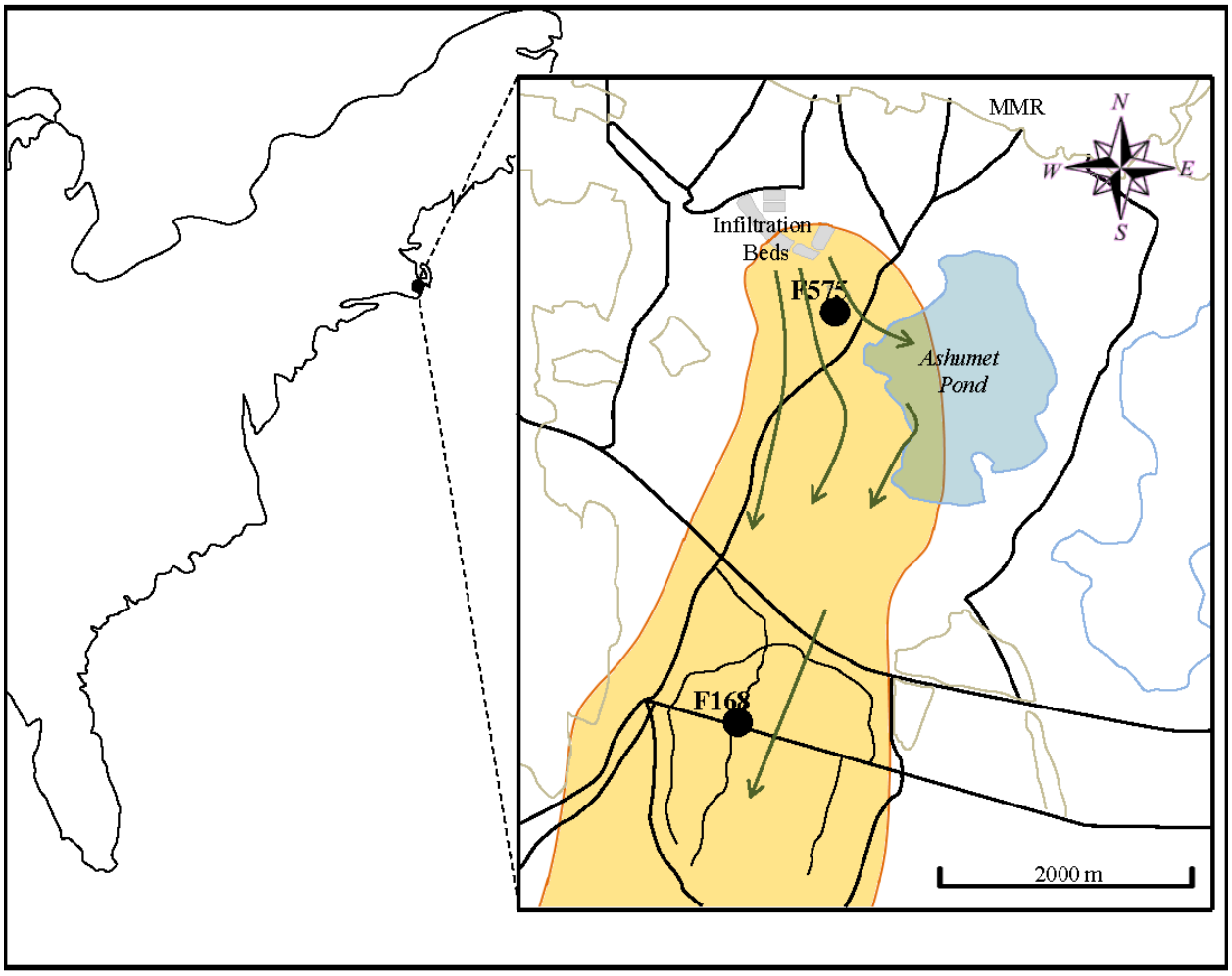

Figure 1. Map of the Cape Cod groundwater plume study site. The orange delineates the plume boundaries and green arrows indicate groundwater flow direction.

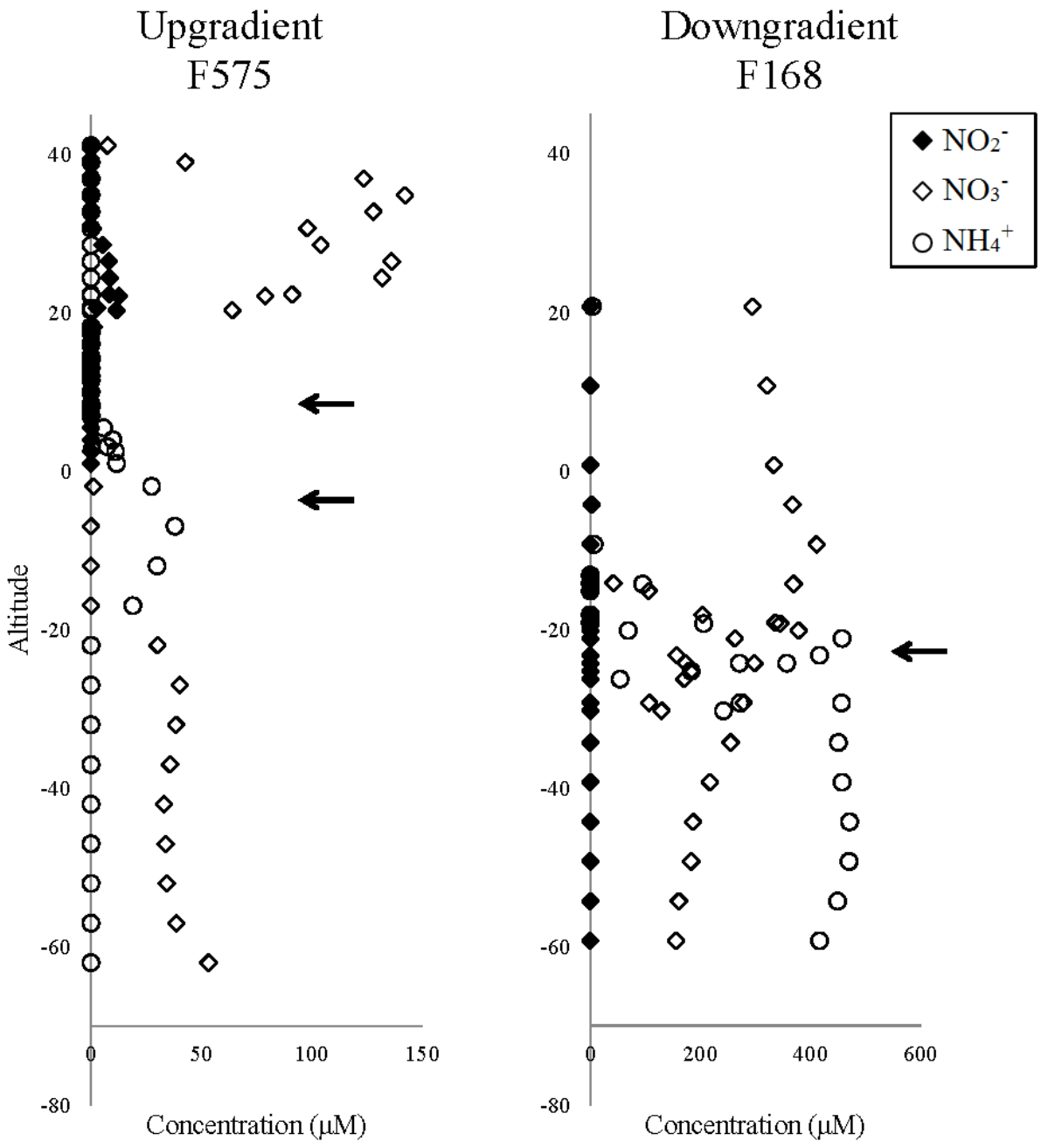

Figure 2. Depth profiles of selected chemical gradients at sites F575 and F168. Arrows denote depths from which sediments and water were collected (Barbaro et al. 2013; Smith et al. per. Com).

Table 1. Experimental treatments by year, depth, and amendment. #MI indicates a nonacetate treatment, and CMI indicates an acetate treatment, with C as the notation for carbon.

Year	Site	Elevation (m alt NAVD88)	Depth ID	Amendment
2011	F575	-2.1 -3.6	D	#MI
			D	CMI
2012	F575	7.6 - 6.1	M	#MI
			M	CMI
2012	F168	-7 - -8	single depth	#MI CMI
2013	F168	-7 - -8	single depth	#MI
				CMI
2013	F168	-7 - -8	single depth	#MI Tracer CMI Tracer

At the upper plume site (F575), sediments from 2 aquifer depths (Deep-D; -2.1 to -3.6 m alt NAVD88, and Middle-M; 7.6 to 6.1 m alt NAVD88) were collected in 2011 and 2012, respectively. Sampling depths that aligned with areas of the geochemical gradient likely to support anammox were chosen (Figure 2). These zones were characterized by a transition in N speciation and/or where denitrification or nitrification had been previously documented that might supply NO_2^- for anammox (Barbaro et al. 2013). The F575 middle depth (M) collected in 2012 had previously shown anammox activity measured during an *in situ* $^{15}NO_2$ tracer injection experiment.

A single depth was sampled at the lower plume site (F168; -7 to 8 m alt NAVD88) in 2012 and 2013. This zone contained high NO_3^- (255 μM) and NH_4^+ (451 μM), but non-detectable NO_2^-, and denitrification was reported to be severely limited by a lack of degradable organic carbon. An *in situ* $^{15}NO_2^-$ tracer experiment performed nearby at the same aquifer depth indicated a dominance of anammox over denitrification.

All sediments were collected using a drilling rig equipped with a sand auger and split spoon sampler. After collection, sediments were stored in headspace free mason jars at 4° C until use in the incubation experiments.

EXPERIMENTAL APPROACH

Natural Abundance Incubations - To determine enrichment factors for various N species involved in anammox and denitrification, we conducted a series of aquifer sediment and groundwater slurry incubations. All incubations were designed as anaerobic. Amendments were made with two primary high concentration combinations (+ NO_2^-, NH_4^+, with/without acetate)

and designated as CMI (+ acetate) and #MI (nonacetate) in order to create environments that favored different amounts of anammox vs denitrification. Downgradient amendments did not include NH_4^+ due to an already existing high background in the groundwater at that site.

Groundwater used in the slurry natural abundance incubations was collected in headspace-free 1 L glass brown bottles from the same plume location and depth as the aquifer sediment. Approximately 10 g of sediment wet-weight was placed into 60 ml serum vials, capped, and immediately evacuated by vacuum to remove any atmosphere introduced during the transfer. The remaining space in the serum bottles was filled with groundwater that had been previously amended according to the treatment and sparged with a gas mixture of argon (1%), nitrogen (80%), and helium (19%). Serum bottles were then crimped with thick butyl stoppers and placed in a roller incubator to continuously mix the slurry during the incubation and minimize any diffusion limitation effects on isotope fractionation.

Time series samples were collected by sacrificing individual serum slurry bottles in triplicate at each time point and analyzed for concentrations and isotopic composition of the NH_4^+, NO_3^-/NO_2^-, and N_2 fractions. Aliquots for different analytes and isotopic analyses were distributed using a peristaltic pump. DIN (frozen), $^{15}NH_4^+$ (frozen), and $^{15}NO_3^-/NO_2^-$ (KOH preserved to pH 12) were 0.2 um filtered. The aliquot for $\delta^{15}N_2$ analysis and N_2 production was not filtered, but was pumped directly into a helium-flushed 30 ml serum vial containing 200 µl of 2N potassium hydroxide (KOH).

Tracer Incubations - $^{15}NO_2^-$ tracer incubations were performed to complement and further investigate the results of the natural abundance fractionation experiments. They were done specifically for three reasons: 1) to further isolate and verify the rates of anammox in the natural abundance set; 2) to determine the efficacy of acetate additions for enhancing denitrification

relative to anammox; 3) to examine the magnitude of DNRA as a potential constraint on interpreting natural abundance changes in NH_4^+ from the natural abundance experiments. Slurries were prepared as described for the fractionation incubations except that 20 g of sediments were used and incubations were done in larger (130 ml) serum bottles. Bottles were incubated for 7 days prior to tracer injection to ensure removal of trace oxygen from the matrix and create a reducing environment. Two treatments were done: 1) $^{15}NO_2^-$ only; and 2) $^{15}NO_2^-$ + acetate. Target concentrations for NO_2^- and acetate were 200 μM and 250 μM, respectively. The ^{15}N isotopic enrichment of $^{15}NO_2^-$ was at >99 At%. Individual vials were sacrificed at intervals to measure concentrations and isotopic composition of the NH_4^+, NO_3^-/NO_2^-, and N_2 and N_2O fractions during the course of the incubations.

ANALYTICAL METHODS

Both natural abundance and tracer incubations used the same analytical methods with respect to N concentrations and isotopic analyses.

NH_4^+ concentrations were measured using the phenol-hypochlorite method (Weatherburn 1967), and NO_3^- and NO_2^- were measured by N-Napthylethylene-diamine azodye formation with and without cadmium reduction, respectively as described by the Greiss Test (Armstrong et al. 1967). N_2O was analyzed on a Gas Chromatograph-Electron Capture Detector (GC-ECD).

$^{15}N_2$ was measured using continuous flow isotope-ratio mass spectrometry (IRMS). The $\delta^{15}N_2$ IRMS analysis used the Gas Bench (GB) interface equipped with a molecular sieve 5A GC column and analyzed at 32° C. $\delta^{15}N_2$ was measured, as well as N_2, O_2, and Ar. Air calibrations of 50, 75, and 120 μl air, were run each day of analysis, and permitted calibration of N_2 area and

N_2/Ar ratios to changes in N_2 mass. All of $\delta^{15}N_2$ were normalized to air $\delta^{15}N$ values using the air standards.

$^{15}NH_4^+$ was measured using an ammonia acid trap diffusion method (Holmes et al. 1999) where ammonium was converted to ammonia gas at pH >11 and trapped as ammonium sulfate on a K_2SO_4 acidified glass fiber filter. The filter was then combusted in a Costech elemental analyzer (EA) and the $\delta^{15}N$ analyzed in a coupled IRMS. All $\delta^{15}NH_4^+$ data were two-point normalized to air $\delta^{15}N$ using known reference materials USGS 40 and 41 L-glutamic acid run concurrently with the ammonium filters.

^{15}N enrichments from the tracer experiments are expressed as ^{15}N mole fractions or, for N_2, individually as the mass of the individual 29 and 30 N_2 isotopologues.

DATA SYNTHESIS

Natural Abundance – The concentration and $\delta^{15}N$ data from the natural abundance experiments was used to determine the effective net enrichment factor (epsilon = ε) according to the Rayleigh model (Eq. 7).

Eq. 7) $$\delta_s = \delta_{s0} + \varepsilon \ln C/C_0$$

Where C is the molar concentration of the substrate at time t, with C_0 being at $t = 0$, δ_s is the isotopic composition at t, with δ_{s0} being at $t = 0$, and ε is the isotopic enrichment factor. (Mariotti et al. 1988).

When δ_s is plotted against the natural log of C, ε in per mille (‰) can be estimated from the slope. Because ε potentially represents the net effect of isotopic changes due to the input and

output in several pools, we also used a finite difference time stepping model, modified from Böhlke (2001) and Böhlke et al. (2002), to assess the nitrogen isotope dynamics in the incubations.

The purposes of this modeling effort were to specifically investigate enrichment factors for anammox, examine the relative effects of varying amounts of anammox, denitrification, and DNRA on the $\delta^{15}N$ values of NO_3^-, NO_2^-, NH_4^+, and N_2, and to help assess the utility of *in situ* distribution of these $\delta^{15}N$ values as a diagnostic indicator of contributions from these reactions to overall aquifer N-cycling. At each time step of the model, an individual N pool (N_t) mass balance was calculated with respect to total N mass, and individually for ^{14}N and ^{15}N. In addition to calculating the micromolar N concentration at each time step, $\delta^{15}N$ values are also calculated at each time step from the individual ^{14}N and ^{15}N concentrations.

The total N in an individual pool (e.g. NO_2^-, or NH_4^+, or N_2) at each time step (N_t) was calculated from N at the previous time-step (N_{t-1}) and the difference between the masses of N entering the pool (N_{in}) from various sources, and N leaving the pool (N_{out}) over the time interval (Eq. 8).

Eq. 8) $$N_t = N_{t-1} + \Sigma N_{ins} - \Sigma N_{outs}$$

Michaelis Mention kinetics was used to parameterize input and output terms, N_{in} and $N_{out,}$ based on:

Eq. 9) $$\frac{Vmax \bullet [\ ]_{t-1}}{Ks + [\ ]_{t-1}} \times \Delta t$$

Where V_{max} and K_s are the maximum rate and half saturation constant, respectively. Brackets denote concentrations either for donor species importing N into the pool of interest, or in the case of reactions removing N, the concentration of the pool of interest. The ^{14}N and ^{15}N inventories at each time step were calculated from equations 10 and 11.

Eq. 10) $$14N_t = 14N_{t-1} + \left[\frac{N_{in,t}}{\left(\propto_{input}\cdot\frac{^{15}N_{donor,t-1}}{^{14}N_{donor,t-1}}+1\right)}\right] - \left[\frac{N_{out,t}}{\left(\propto_{output}\cdot\frac{^{15}N_{t-1}}{^{14}N_{t-1}}+1\right)}\right]$$

Eq. 11) $$15N_t = 15N_{t-1} + \left\{\frac{N_{in,t}}{\left[\left(\propto_{input}\cdot\frac{^{15}N_{donor,t-1}}{^{14}N_{donor,t-1}}\right)^{-1}+1\right]}\right\} - \left\{\frac{N_{out,t}}{\left[\left(\propto_{output}\cdot\frac{^{15}N_{t-1}}{^{14}N_{t-1}}\right)^{-1}+1\right]}\right\}$$

Finally, at each time step the ^{14}N and ^{15}N inventories are used to calculate a $\delta^{15}N$ value for each N species:

Eq. 12) $$\delta 15N = 1000 \cdot \left[\left(\frac{^{15}N_t}{^{14}N_t}\right)\cdot 272 - 1\right]$$

Best model fits to measured concentration and $\delta^{15}N$ data for NO_3^-, NO_2^-, NH_4^+, and N_2 were achieved by adjusting V_{max}, K_s, and α values for each reaction. These parameters were constrained by literature values and by the following additional constraints established from the tracer incubations and/or field tracer injections: 1) the DNRA to (amammox + denitrification) ratio was ≤ 0.25; 2) the anammox to denitrification ratio was ≤ 0.4; 3) all alphas were ≥ 0.970 and ≤ 1.0.

Tracer – The following equations were used to calculate anammox (Eq. 13), denitrification (Eq. 14), and DNRA (Eq. 15) from data generated in the tracer experiments (Thamdrup and Dalsgaard 2002).

Eq. 13) $N_{2\ anammox} = [^{29}N_2 + 2 \times (1 - (1/MF_{NO2})) \times {}^{30}N_2]/MF_{NO2}$

Eq. 14) $N_{2\ denitrification} = {}^{30}N_2/(MF_{NO2})^2$

Eq. 15) $DNRA = [(MF_{NH4} - R) \times NH_4^+{}_{tot}]/MF_{NO2}$

Where *MF* denotes the mole fraction of ^{15}N in NO_2^- or NH_4^+ pools. $NH_4^+{}_{tot}$ refers to mass of all NH_4^+ present in the incubation. $^{29}N_2$ and $^{30}N_2$ refer to the production rates of mass 29 and 30 N_2 isotopologues, respectively.

RESULTS

NATURAL ABUNDANCE FRACTIONATION EXPERIMENTS

Upgradient F57 Site - The F575 experiments were performed with sediments collected from two depths: 1) the zone of -2.1 - -3.6 m alt NAVD88 (D) characterized by moderate NH_4^+ elevation; and 2) the zone of 7.6 – 6.1 m alt NAVD88 (M) located at the base of the NO_3^- region. During the 2011 F575 D zone sediment incubations, the nonacetate #MI treatment (NH_4^+ and NO_2^-) showed NO_3^- drawdown prior to that of NO_2^- (Figure 3.a). Complete NO_3^- and NO_2^- removal occurred by day 18 and day 31, respectively. The NH_4^+ concentration also decreased initially from 80 μM to a minimum of 55 μM at day 31, and then increased to 67 μM by day 47. The net total loss of NH_4^+ during the incubation was 13 μM, or about 20% of the initial aqueous concentration (Figure 3.a). The $\delta^{15}N$ of all DIN species steadily increased during the incubation. Large enrichments (up to 30‰) were measured in $\delta^{15}NO_3^-$ and $\delta^{15}NO_2^-$, with a 4‰ increase in $\delta^{15}NH_4^+$ over the same duration (Figure 3.b). The end product of denitrification and/or anammox, N_2, showed a net increase of 66 μM in 47 days. The rate of production was greatest between days 0 and 18 (2 μM/day). The pattern of $\delta^{15}N_2$ was characterized by an initial $\delta^{15}N_2$ depletion of 0.5‰, followed by a rise in the $\delta^{15}N_2$ as the enriched NO_2^- found later in the incubation was converted to N_2 (Figure 3.c).

The addition of acetate (CMI) to the D zone sediments induced removal rates of NO_3^- and NO_2^- that appeared at least 2-3 times faster than those of the #MI treatment. Similar to the nonacetate treatment, NO_3^- consumption preceded NO_2^- loss. Similarly, NH_4^+ also showed an initial rapid drop to a minimum of 58 μM at day 7. Unlike the nonacetate treatment, this occurred in the presence of trace O_2. This was followed by a leveling out of ammonium,

amounting to a loss on the order of 25% of the initial NH_4^+ concentration (Figure 3.d). Isotopic enrichments in CMI showed similar patterns to those of #MI, in $\delta^{15}(NO_{3+2})$ and $\delta^{15}NO_2^-$ initial ‰, and in terms of the magnitude of enrichment in the NO_3^- and NO_2^- over time, but the isotopic shifts occurred faster in the CMI due to the faster NO_3^- and NO_2^- consumption rates (Figure 3.e). The $\delta^{15}NH_4^+$ initially rose by 4‰ during the period of trace O_2 (>10 μM) but was then invariant for the remainder of the experiment. N_2 production in CMI was 50% higher than #MI, and showed a marked plateau after day 18 after all the NO_3^- and NO_2^- had been drawn down. The greatest N_2 production rate occurred between day 0 and day 4 (10 μM/day), and was coincident with the initial drop in $\delta^{15}N_2$ as the pool received fractionated N from NO_2^-. A rebounding enrichment in $\delta^{15}N_2$ of 1-1.5‰ followed the initial depletion to plateau values that were 0.3‰ higher than the initial $\delta^{15}N_2$ (Figure 3.f).

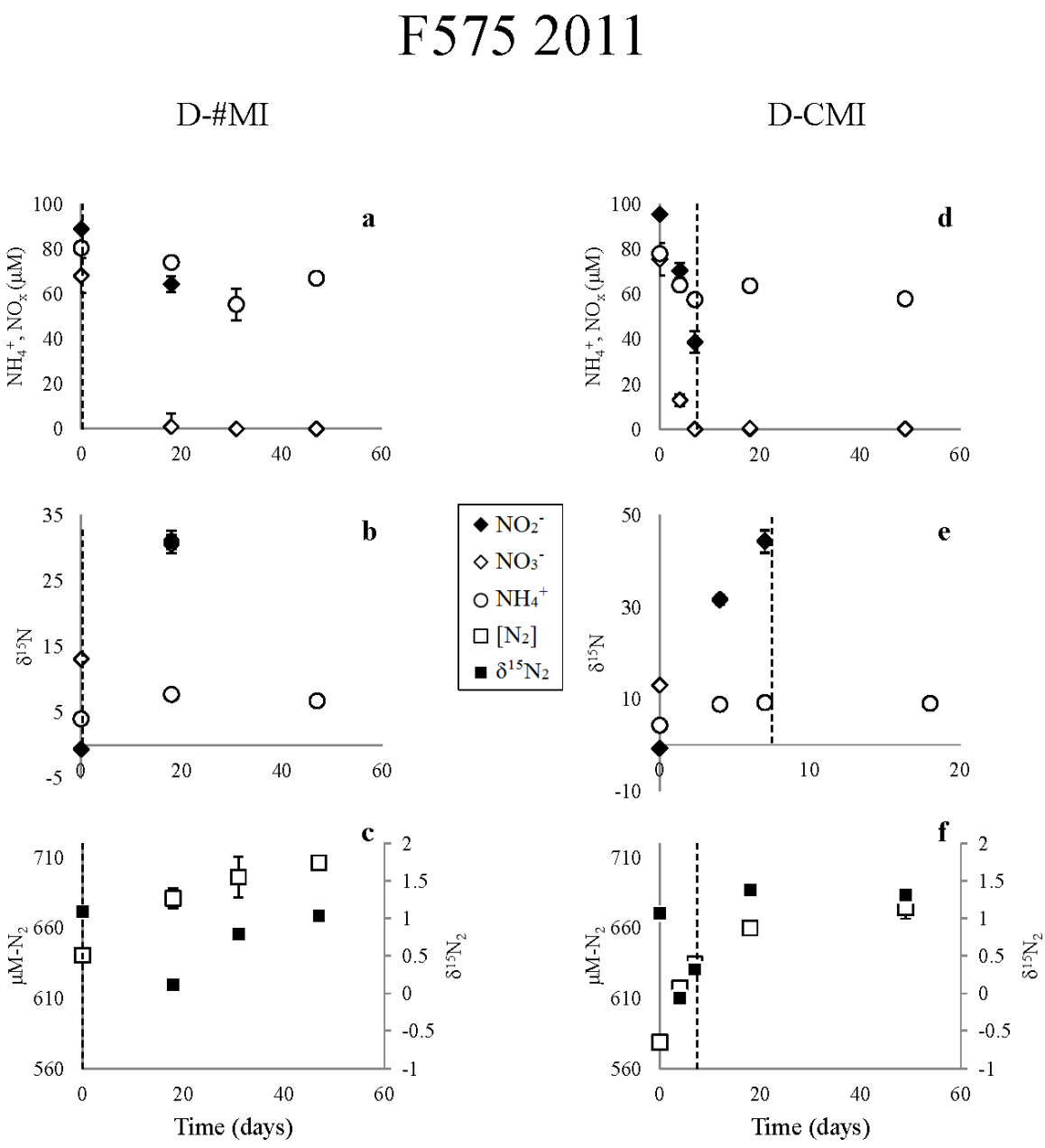

Figure 3. N concentrations and isotopes for incubations using upper plume F575 deep (D) sediments collected and incubated in 2011. Nonacetate (panels a, b, c) and acetate (panels d, e, f) are shown. The dashed line indicates the time at which trace oxygen was gone from the incubation. Standard deviations are reported for all data, but when not seen, the error bars are smaller than the size of the symbol.

F575 Zone M sediments were subject to the same NO_2^- and NH_4^+ with/without acetate treatments as Zone D. Target initial concentrations for NO_2^- were raised to 200 μM, and more sampling times were added. In the #MI treatment, ambient NO_3^- of 27 μM was quickly reduced below 10 μM by day 4 and completely consumed by day 21. There was a lagged NO_2^- removal that occurred during the trace O_2 period, which then accelerated between days 10 and 20, and continued until all NO_2^- was consumed by day 40. NH_4^+ dropped initially by 20% by day 4 during the trace oxic period, and was then invariant for the remainder of the experiment. Up to 8 μM N_2O was detected at day 17 during NO_x drawdown (Figure 4.a). Large $\delta^{15}N$ enrichments in excess of 45‰ were measured in NO_2^- and NO_3^- during the incubation. The $\delta^{15}NH_4^+$ values initially rose by 4‰ up until day 9 during the trace O_2 period, but then plateaued between 8 and 9‰ for the remainder of the incubation (Figure 4.b). N_2 production lagged for the first week of the incubation, similar to the lag in NO_2^- loss, followed by increases approximately equivalent to the amount of NO_2^- loss. The $\delta^{15}N_2$ showed the characteristic J-shaped pattern ("J-curve") of initial isotopic depletion (to -1‰) commensurate with initial N_2 production, followed by a rise in $\delta^{15}N_2$ towards the latter part of the incubation (Figure 4.c). The final $\delta^{15}N_2$ was 0.3 to 0.5‰ higher than the starting $\delta^{15}N_2$.

The CMI treatment in the M zone sediments showed a similar behavior for NO_3^-, NO_2^-, and NH_4^+ concentrations and isotopes, albeit with a 2 day shorter lag in NO_3^- and NO_2^- loss. N_2O concentration reached a peak concentration of 5 μM-N occurring at 20 days (Figure 4.d). This was concurrent with the point of 50% loss in NO_2^-, as well as the start of $\delta^{15}N_2$ rise after its minimum. As observed in the #MI treatment, $\delta^{15}NO_3^-$ and $^{15}NO_2^-$ increased linearly over time to >45‰, the $\delta^{15}NH_4^+$ rose by 7‰ and plateaued, and the "J curve" in the $\delta^{15}N_2$ was contemporaneous with N_2 production (Figure 4.e, f). CMI however yielded 15 μM more N_2 than

#MI, with the amplitude of the $\delta^{15}N_2$ J-curve (max $\delta^{15}N_2$-min $\delta^{15}N_2$) was 0.5‰ larger than that measured for #MI.

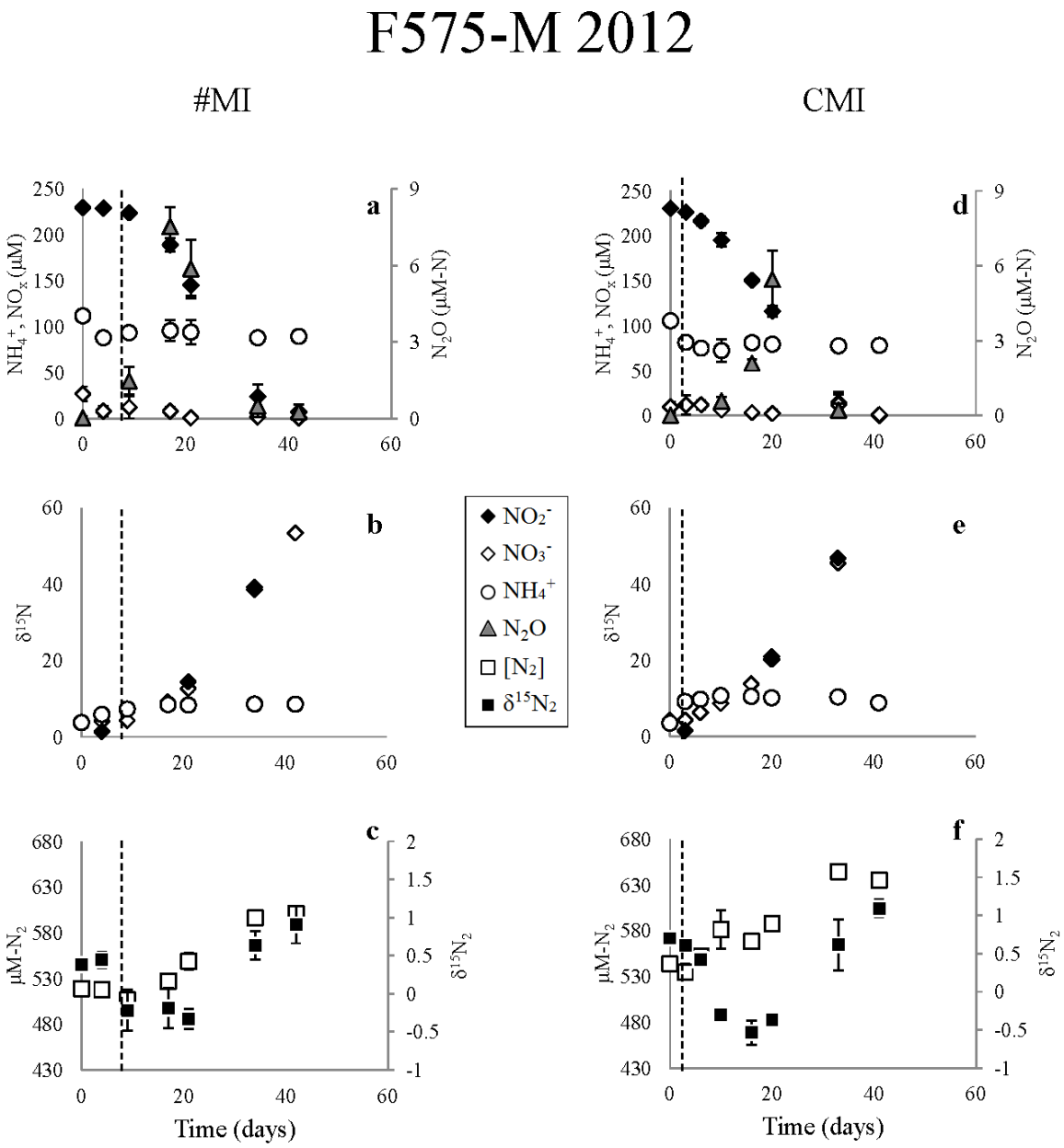

Figure 4. N concentrations and isotopes for incubations using upper plume F575 mid-depth (M) sediments collected and incubated in 2012. Nonacetate (#MI, a, b, c) and acetate (CMI, d, e, f) treatments are shown in vertical panels. Dashed lines indicate the end of the trace oxic period. N_2O concentrations are shown in combination with other DIN species concentrations.

Downgradient F168 Site - F168 treatments used sediments and groundwater from one depth (-7-8 m alt NAVD88), characterized by the presence of high NO_3^- and NH_4^+ concentration. Treatments were identical to those used with the upgradient site. Overall, rates for #MI were slower than those measured at F575, but the CMI rates for both sites were similar (Figure 3-6). In the 2012 #MI experiment, both NO_3^- and NO_2^- increased in concentration (by 43 and 57μM, respectively) within the first 14 days during a period when trace O_2 was present in the incubation. Both concurrently decreased to residual levels (<6 μM) by day 57, but were never fully consumed by the end of the incubation. The #MI NH_4^+ initially decreased by 25% during the trace oxic period, but fluctuated over time between 60 and 95% of its initial concentration (265 μM). Net NH_4^+ loss was 107μM. N_2O was not present until after day 21, when it accumulated to a maximum of 33 μM-N by day 57 (Figure 5.a).

Because NO_3^- and NH_4^+ were present in high concentrations at this site, initial isotopic enrichments for both represent background concentrations. $\delta^{15}NO_{3+2}$ and $\delta^{15}NO_2^-$ enrichments remained invariant around 10‰ and 2‰ until day 14, when they began to increase as both NO_3^- and NO_2^- were consumed. Enrichments up to 37‰ were measured in both pools by day 34. $\delta^{15}NH_4^+$ fluctuated only between 16 and 17‰ (Figure 5.b) for the entire incubation. N_2 production occurred throughout the incubation, for a yield of 126 μM. The initial drop in $\delta^{15}N_2$ was slow and reached its minimum of -0.54‰ on day 34. The subsequent "J-curve" rebound in $\delta^{15}N_2$ reached a final enrichment at 1.8‰ greater than its initial value (Figure 5.c).

The CMI treatment showed similar behavior to the #MI in concentration but reaction rates were approximately twice those measured in #MI. NO_3^- drawdown had a steeper slope than that of NO_2^- and both were completely removed by day 33. NH_4^+ fluctuated widely within a range of 121 μM during the incubation but yielded a small net decrease of 22 μM. N_2O

production did not occur until after day 7, with a sharp rise to a maximum of 7 μM-N within 5 days. It fell steadily to 0 by day 33 (Figure 5.d).

The $\delta^{15}NO_{3+2}$ and $\delta^{15}NO_2^-$ isotope values increased by up to 55‰, at which point NO_2^- and NO_3^- were no longer detectable. Despite a small initial rise in $\delta^{15}NH_4^+$ of 1‰, the value varied within the range of 16-18‰ throughout the incubation (Figure 5.e). Rapid N_2 production in the first 14 days plateaued by day 30 and yielded a total of 152 μM. The rapid N_2 production was accompanied by rapid depletion of $\delta^{15}N_2$, followed by the expected rise as the remaining NO_2^- was reduced. At the end of the incubation, maximum $\delta^{15}N_2$ was1.5‰ greater than the initial (Figure 5.f).

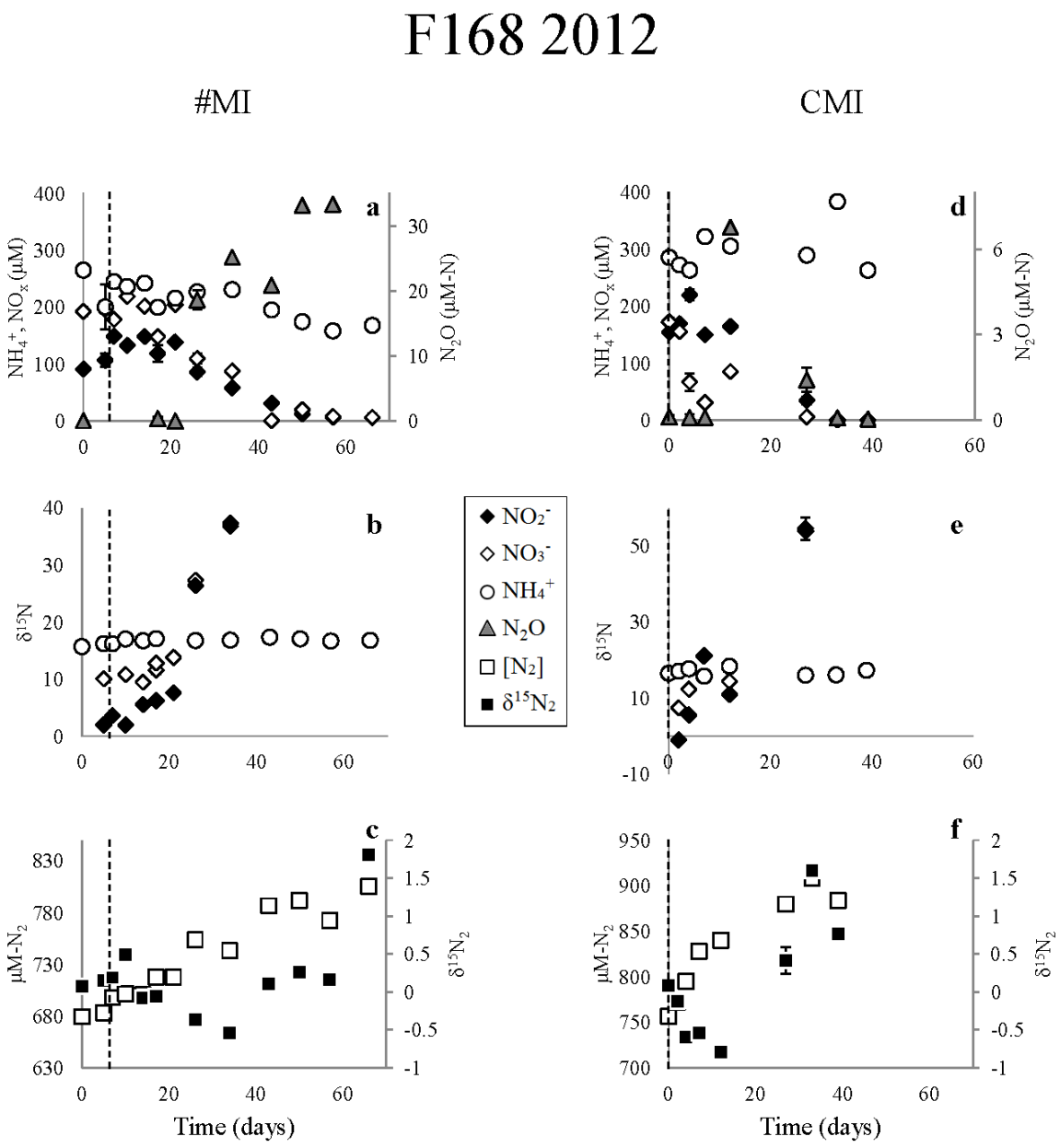

Figure 5. N concentrations and isotopes for incubations using lower plume F168 sediments collected and incubated in 2012. Nonacetate (#MI) and acetate (CMI) treatments are shown in vertical panels. Dashed lines indicate the end of the trace oxic period. N_2O concentrations are shown in combination with other DIN species concentrations.

F168 sediments collected in 2012 were used again in a repeat incubation experiment in 2013 to better constrain the enrichment factors. The same treatments were used. The nonacetate #MI treatment showed an extremely low NO_x reduction and N_2 production rate relative to the 2012 experiment when sediments were fresher. A low rate of NO_3^- loss was accompanied by a near quantitative rise in NO_2^-. NO_2^- did not decrease throughout the entire incubation. NH_4^+, which decreased from day 0 – 9, afterwards slowly increased to a value near the initial NH_4^+ concentration of 368 μM by the end of the sampling period (Figure 6.a).

An initial $\delta^{15}NO_{3+2}$ value of 7‰ in the #MI treatment rose steadily throughout the experiment at a rate of about 0.13‰ per day to a maximum enrichment of 20‰. $\delta^{15}NO_2^-$ was initially lighter than $\delta^{15}NO_{3+2}$, but matched its enrichment by day 21. $\delta^{15}NH_4^+$ initially decreased during the trace O_2 phase, but varied less than 1‰ throughout the course of the experiment (Figure 6.b). Very slow linear N_2 production was characterized by a slow linear $\delta^{15}N_2$ depletion of 1‰ during the entire incubation. Insufficient conversion of NO_2^- occurred to cause a rebound in the $\delta^{15}N_2$ as observed in the other incubations (Fig 6.c).

In the corresponding CMI treatment, faster rates relative to #MI resulted in fully consumed NO_3^- within the first 3 days and NO_2^- by day 50. These NO_x reduction rates were on par with the 2012 CMI experiment, indicating that the very low rates in the 2013 #MI relative to 2012 were probably related to less available carbon in older unamended sediments. NH_4^+ varied within an 89 μM range, but showed a pattern of initial decrease while NO_2^- was consumed, and was followed by rising NH_4^+ until the end of the incubation (Figure 6.d).

$\delta^{15}NO_{3+2}$ showed strong enrichments up to 80‰ during the rapid reduction of NO_2^- and NO_3^-. $\delta^{15}NH_4^+$ showed a small 1‰ enrichment between days 0-3, followed by little to no variation (±0.3‰) for the remainder of the incubation (Figure 6.e). The pattern of N_2 was

characteristic of the other CMI incubations, with rapid N_2 production followed by a plateau after all NO_x had been consumed. The general "J-shaped" curve was evident in the $\delta^{15}N_2$, albeit with some higher variance than observed in the other treatments. The $\delta^{15}N_2$ dropped to 0.5‰ and eventually rebounded to a maximum of 2‰ by the end of the incubation (Figure 6.f).

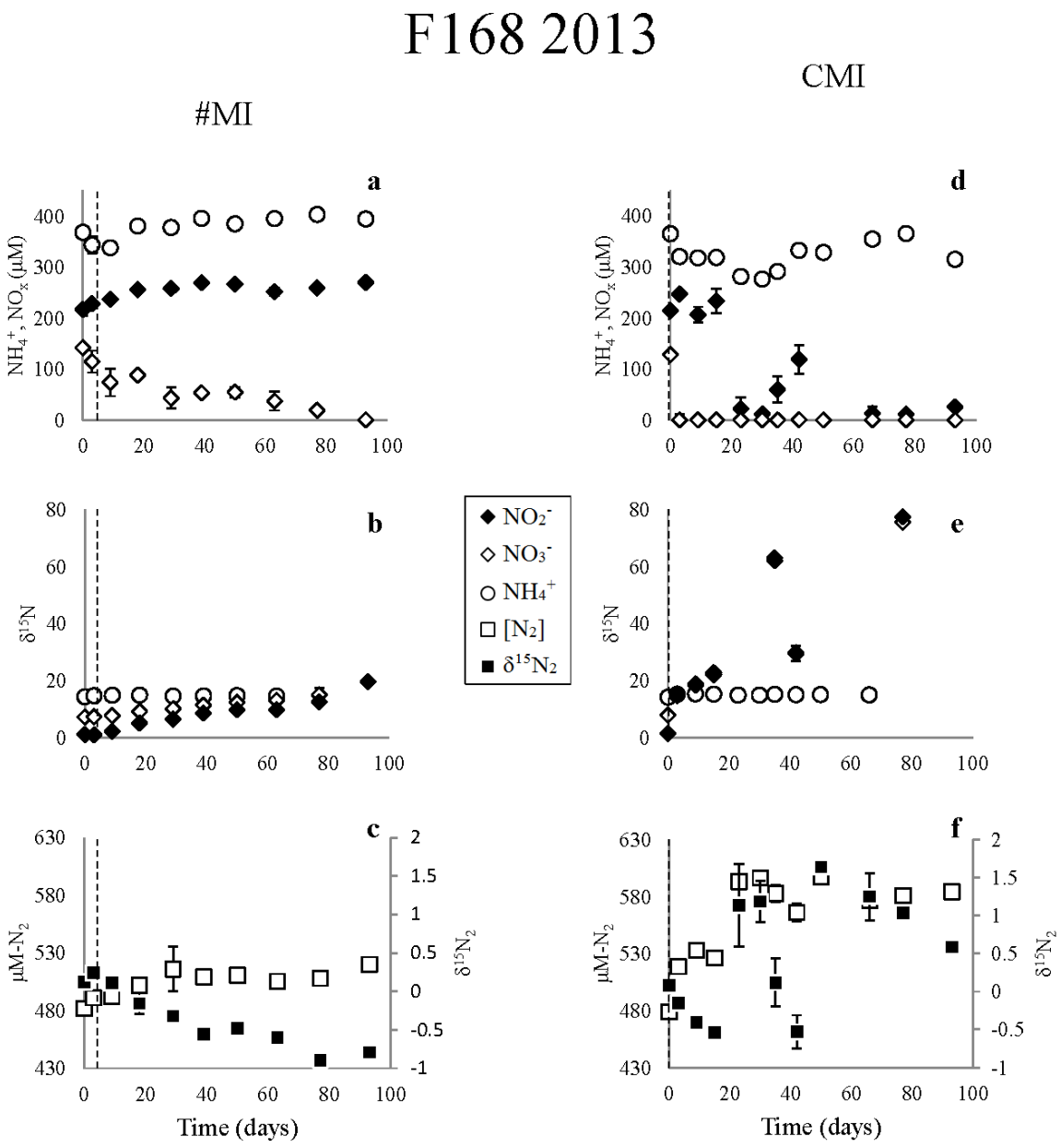

Figure 6. N concentrations and isotopes for incubations using lower plume F168 sediments collected and incubated in 2012. Nonacetate (#MI) and acetate (CMI) treatments are shown in vertical panels. Dashed lines indicate the end of the trace oxic period. N_2O concentrations are shown in combination with other DIN species concentrations.

Rayleigh-derived Apparent Isotope Enrichment Factors – Rayleigh plots relating change in N species concentration to change in $\delta^{15}N$ were constructed for the O_2 free portions of all natural abundance incubations. The Rayleigh plots for the upper plume F575 were characterized by high NO_2^- and low NO_3^-, so NO_{3+2} enrichment factors derived from ^{15}N analysis with *P. aurofaciens* were similar to those for NO_2^- only derived from ^{15}N analyses using *S. nitritireducens.*

All experiments showed good fits ($r^2 \geq 0.82$) for the NO_{3+2} and NO_2^- data in the majority of treatments. The NO_{3+2} enrichment factors were within 1-2‰ of the NO_2^- enrichment factors (Figure 7-8). For the D zone sediments, nonacetate NO_{3+2} and NO_2^- fractionations did not generate good fits to yield enrichment factors ($p > 0.05$). In comparison, plus acetate treatments yielded enrichment factors of -23 and -21‰ for NO_{3+2} and NO_2^- respectively (Table 2). For the M zone sediments, the #MI treatment yielded 3-4‰ magnitude greater enrichment factors for NO_{3+2} and NO_2^- (ε = -19‰) relative to the deep sediments, but the acetate CMI treatments were identical between the two sediment types (ε = -21‰) (Table 2). For ammonium, very poor fits to the Rayleigh model were found for all treatments in both zones when all $\delta^{15}NH_4^+$ and concentration data were examined (Figure 9). The poor fits were likely due to both small changes in NH_4^+ concentration, and to competing reactions/sediment-water exchanges at different times of the incubation (e.g. aerobic ammonium oxidation near the start of the incubation fueled by trace O_2 at greater than 10 μM entrained into the serum bottle). NH_4^+ isotope and concentration data analyzed after trace O_2 removal and the establishment of reducing conditions showed no improvement in the Rayleigh fits for #MI treatments (Figure 9.a-b). CMI $\delta^{15}NH_4^+$ exhibited fits ($r^2 > 0.72$, $p < 0.05$) with enrichment factors of -15 and -16‰ for D and M

zone sediments, respectively during the presence of trace O_2 (suggestive of aerobic ammonium oxidation), but poor Rayleigh fits remained after O_2 fell below 10 μM (Figure 9.a-b).

Rayleigh plots at the downgradient F168 site for 2012 and 2013 experiments yielded good fits for all NO_{3+2} and NO_2^- concentration and isotope data ($r^2 \geq 0.85$) (Figures 7-8) . Here there was high background NO_3^- in addition to the added NO_2^-, so unique enrichment factors for NO_3^- and NO_2^- reduction could be derived from the measured NO_{3+2} and NO_2^- $\delta^{15}N$ analyses. This was possible for the #MI treatments where NO_3^- remained long enough to capture changes in concentration, but not in the CMI treatments where NO_3^- was consumed faster than the timescale of sampling. In both the 2012 and 2013 experiments, the #MI treatment yielded enrichment factors for NO_2^- reduction that were 8-12‰ magnitude greater than NO_3^- reduction, yet the magnitudes of the enrichment factors were very different for each species between years. The faster 2012 experiment isotope effects for NO_2^- and NO_3^- loss were -27 and -8‰ respectively (Figure 7.c, d). The 2013 experiment, where low rates of NO_3^- loss were accompanied by relatively little loss of NO_2^-, yielded very large apparent enrichment factors for NO_2^- and NO_3^- of- 47 and -35‰. These enrichment factors in the #MI treatments represent the net effect of both the NO_3^- and NO_2^- reductions. When the NO_{3+2} enrichment factors are considered for #MI, 2012 and 2013 show similar values of -17 and -19‰ despite the large difference in reaction rates. These enrichment factors were similar to values to those found in the #MI F575 experiments. Similar to the upgradient F575 experiments, the $\delta^{15}NH_4^+$ Rayleigh plots did not yield good fits ($r^2 \leq 0.06$). Separating data into a post-O_2 removal period did not improve the fits during the O_2 free period, but did permit estimation of an enrichment factor for NH_4^+ loss during the trace O_2 period in F168 2012 #MI when aerobic ammonium oxidation was likely operating.

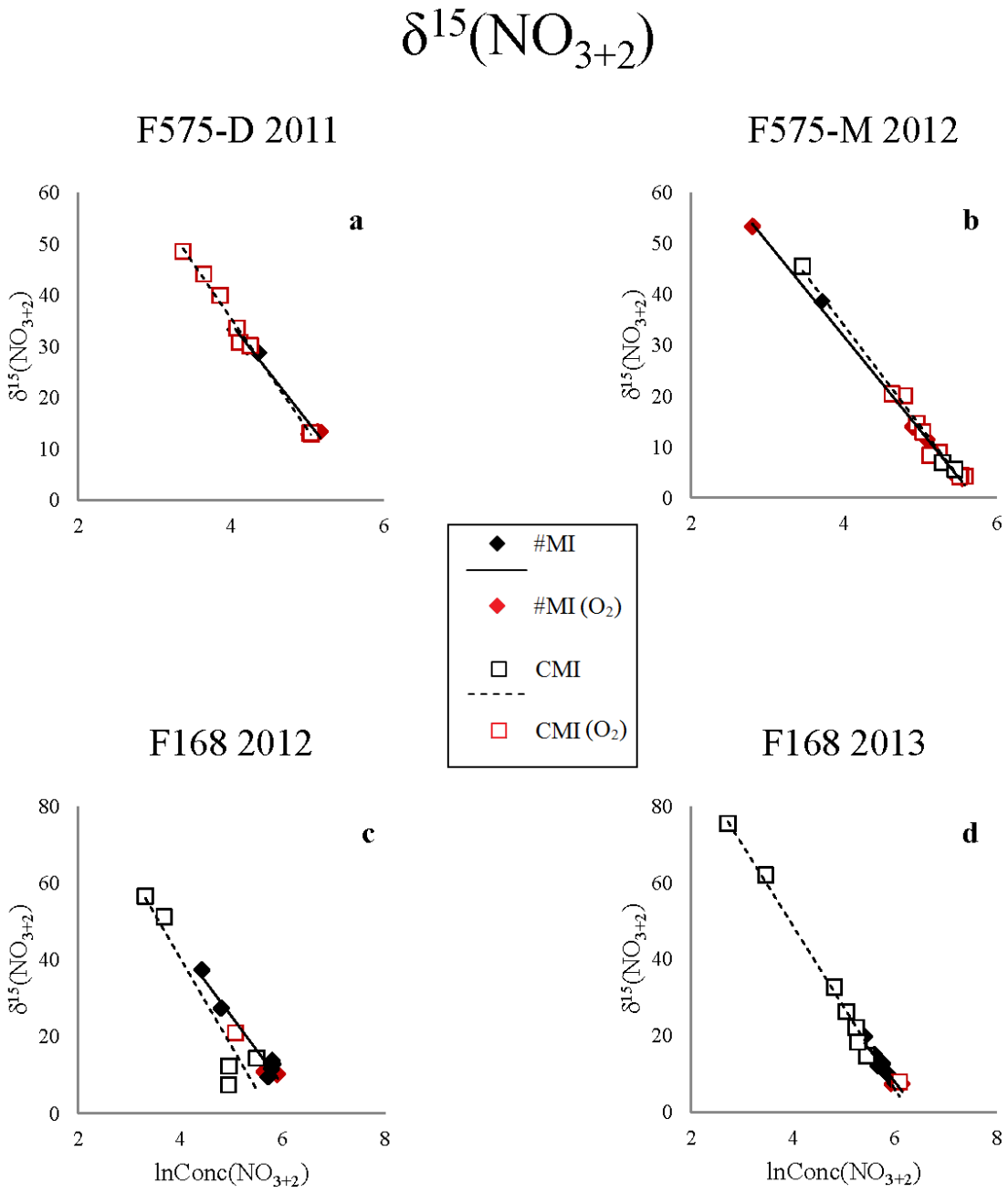

Figure 7. Rayleigh plots for combined $\delta^{15}(NO_{3+2})$ for all four natural abundance experiments. Effective enrichment factors (ε) for NO2+3 reduction were estimated from the slope of these plots and summarized in Table 2. Red symbols indicate data collected during a period of trace oxygen in the incubations.

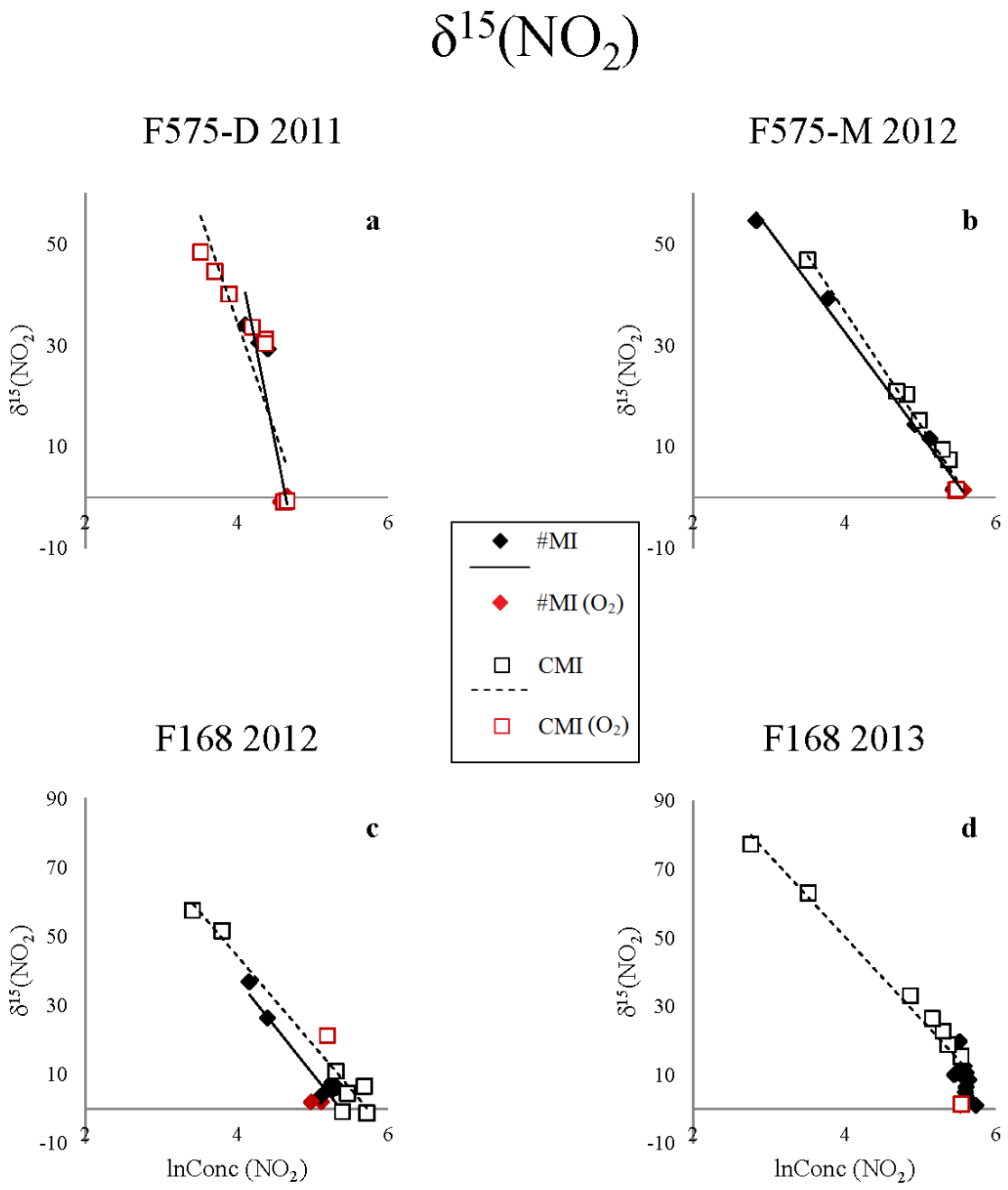

Figure 8. Rayleigh plots for $\delta^{15}NO_2^-$ for all four natural abundance experiments. Effective enrichment factors (ε) for NO_2^- reduction were estimated from the slope of these plots and summarized in Table 2. Red symbols indicate data collected during a period of trace oxygen in the incubations.

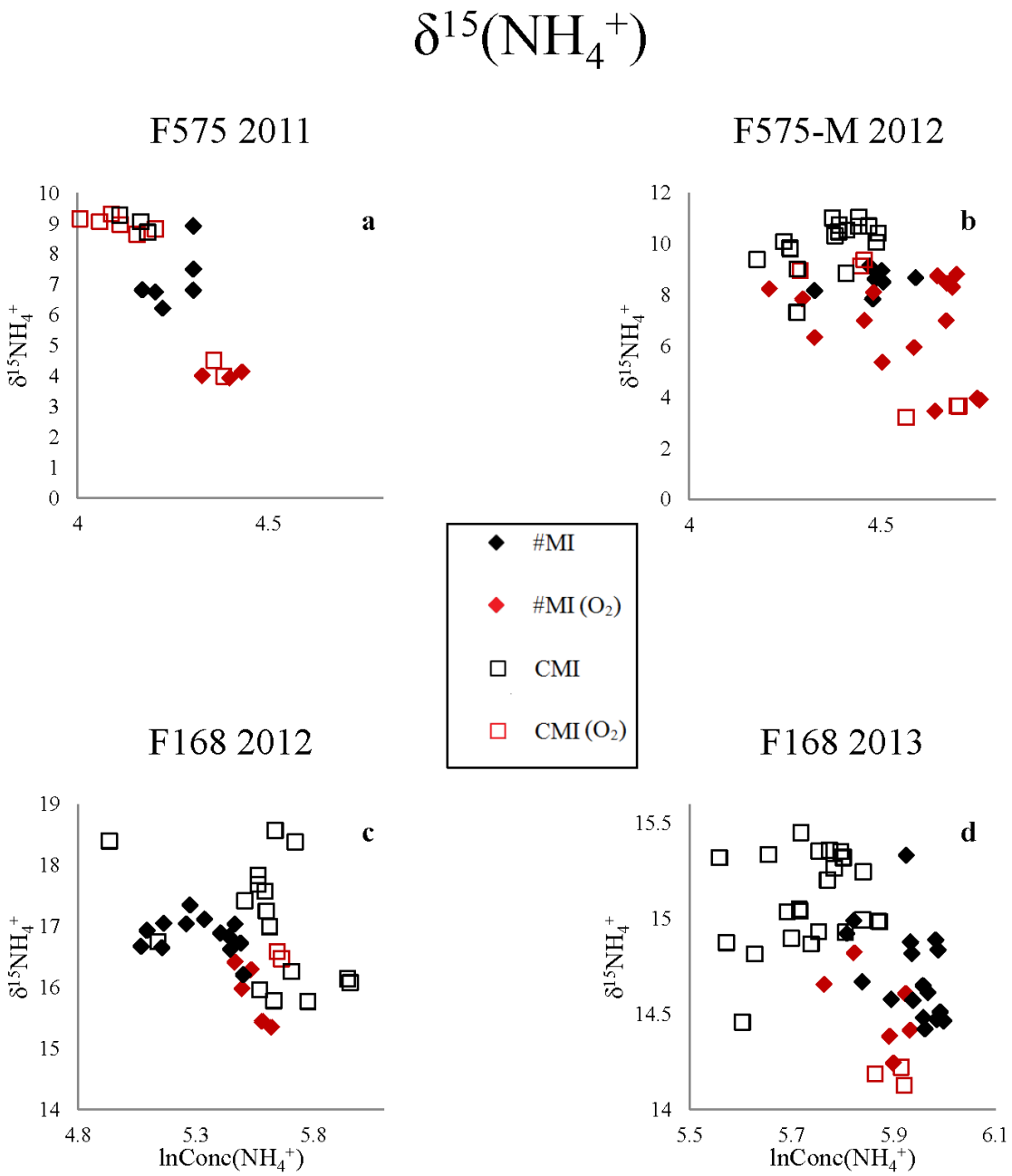

Figure 9. Rayleigh plots for $\delta^{15}NH_4^+$. Effective enrichment factors (ε) could not be estimated from these data with the exception of F575-D-CMI, F575-M-#MI, and F168-#MI during the trace O_2 period. These enrichment factors likely reflect a dominance of aerobic ammonium oxidation and not anammox. Red symbols indicate data collected during a period of trace oxygen in the incubations.

Table 2. Apparent enrichment factors (epsilon: ε) imprinted from net N loss on discrete DIN pools. Where $\varepsilon = (\alpha - 1) \times 1000$, and α is the fractionation factor defined by the ratio of the rate constants ($^{15}k/^{14}k$) for a reaction. Isotope effects for NO_3^-, NO_2^-, and NO_{3+2} are for the period after trace O_2 has been consumed. Enrichment factors reported for NH_4^+ are generated from aerobic periods, and are denoted in red with an asterisk. With the exception of F168 2013 NO_2^-, only enrichment factors where $p < 0.05$ and substrate concentration decreases by at least 20% are shown.

Experiment	Treatment Name	Substrate	-ε	r^2	Standard Error	p
F575 2011	D-CMI	NO_{3+2}	23	0.9734	1	<0.001
		NO_2^-	21	0.9963	1	<0.001
		NH_4^{+*}	15	0.8560	3	<0.001
F575 2012	#MI	NO_{3+2}	19	0.9982	<1	<0.001
		NO_2^-	19	0.9968	1	<0.001
	CMI	NO_{3+2}	21	0.9881	1	<0.001
		NO_2^-	21	0.9966	1	<0.001
		NH_4^{+*}	16	0.7167	5	0.033
F168 2012	#MI	NO_{3+2}	17	0.9810	1	<0.001
		NO_3^-	8	0.9342	1	0.007
		NO_2^-	27	0.9488	3	<0.001
		NH_4^{+*}	7	0.7841	2	0.046
	CMI	NO_{3+2}	22	0.9339	4	0.034
		NO_2^-	26	0.9667	2	<0.001
F168 2013	#MI	NO_{3+2}	19	0.9395	2	<0.001
		NO_3^-	35	0.8554	5	<0.001
		NO_2^-	47	0.3195	24	0.089
	CMI	NO_{3+2}	22	0.9943	1	<0.001
		NO_2^-	22	0.9964	1	<0.001

^{15}N Tracer Incubation Experiment – F168 – In the #MI (nonacetate) treatment, ambient NO_3^- (71 μM) was removed by day 31. NO_2^- concentration decreased by 17% for a net loss of 41 μM. The ^{15}N enrichment of the added NO_2^- showed an isotope dilution during the incubation from 96 at% to 77 at% over 29 days (Figure 10). N_2 production was not observed until day 31, but detectable mass 29 and mass 30 enrichments were measured as early as day 17 (mole fractions 0.020 and 0.051, respectively). The highest 29 and 30 mole fractions observed were 0.036 and 0.070 at day 31. Calculated anammox and denitrification rates (eq. 13, 14) within the last 12 days were 5.5 and 19 nmoles N/g sed/day respectively. Anammox accounted for 28% of the total N_2 production (Figure 10). Tracer incorporation into NH_4^+ was observed and the $\delta^{15}NH_4^+$ increased by 747‰ over the duration of the incubation (Figure 10). The calculated DNRA rate (eq. 15) was 1 nmoles-N/g sed/day. DNRA accounted for 4% of the NO_2^- loss in the #MI treatment.

In the acetate treatment, NO_3^- drawdown was complete by day 3. NO_2^- was also fully removed by day 3, undergoing little change for the first day, but yielding a rate of 236 μM/day between 2 and 3 days. $^{15}NO_2^-$ enrichment showed an isotope dilution from 99 at% to 19 at% by the last sampling point when <2 μM NO_2^- remained. Denitrification, anammox, and DNRA rates all increased in the presence of acetate, but the proportions of these reactions to each other differed relative to the #MI treatment. N_2 production was observed beginning at 0.7 days post injection. Mass 29 and 30 enrichments were first measured at 2 days with mole fractions of 0.014 and 0.020 that increased to 0.088 and 0.103 by the end of the incubation (day 4). Anammox and denitrification rates (eq. 13, 14) were calculated as 24 and 555 nmoles-N/g sed/day respectively, with anammox responsible for 4% of the total N_2 production. A smaller amount of ^{15}N tracer in $NH4^+$ was measured relative to #MI, albeit in 1/6 the amount of

incubation time, and enrichment reached a maximum of 218‰ (Figure 10). The calculated DNRA rate (eq. 15) was 3 nmol-N/g sed/day. DNRA accounted for <2% of the NO_2^- loss in the CMI treatment.

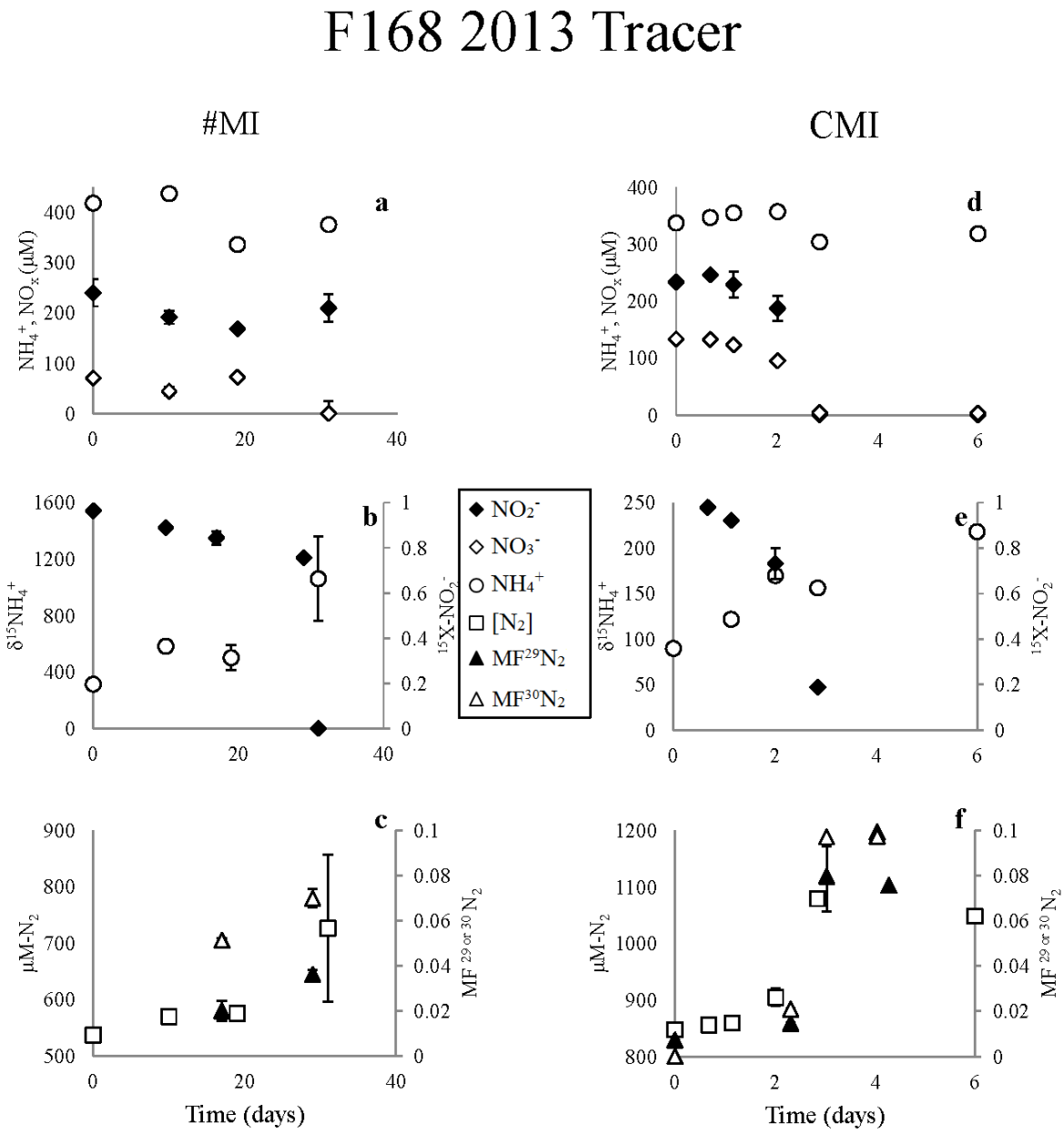

Figure 10. Results from the F168 tracer experiment. DIN concentrations and isotopes are shown in panels a-d. N_2 concentrations and mole fractions (MF) of isotopologues ($^{29}N_2$, $^{30}N_2$) are shown panels e and f. No trace O_2 was measured at any timepoints.

DISCUSSION

Results from our natural abundance and tracer incubations yielded five findings: 1) denitrification and anammox co-occur in aquifer sediments, albeit at relatively low rates; 2) addition of labile organic carbon in the form of acetate shifts the denitrification/anammox ratio very strongly in favor of denitrification; 3) no distinguishable NO_2^- or NO_3^- isotope fractionation patterns could be discerned that were unique or diagnostic of specifically anammox or denitrification; 4) the use of $\delta^{15}NH_4^+$ as a diagnostic for anammox is potentially confounded by large NH_4^+ pool size and aqueous/sediment exchange; 5) isotope modeling demonstrates that the observed isotope dynamics can be achieved with or without anammox in conjunction with denitrification.

CO-OCCURRENCE OF DENITRIFICATION AND ANAMMOX

There are few reported anammox measurements in groundwater (Clark et al. 2008; Moore et al. 2011, Robertson et al. 2012). The rates of N_2 production observed here in the natural abundance incubations from the upper and lower plume, and the tracer-based rate measurements of denitrification and anammox in the lower plume, together indicated co-occurrence of both reactions. The rates measured in this study, which ranged between from 5.5-24 nmoles N/g sed/day for anammox and 19-555 nmoles N/g sed/day for denitrification, were comparable with other laboratory incubations of water and whole sediments collected from this site (Hyun et al. 2013), but 20-fold higher than *in situ* rates calculated following a $^{15}NO_2^-$ groundwater injection at this site (Smith et al. 2013). These incubation-derived rates relative to *in situ* were also faster than what would be predicted based upon modeled plume scale N_2

production during plume transport (Smith et al. 2004; Böhlke et al. 2006; Smith et al. 2013). This apparent enhancement in the lab incubations could have been due to increased incubation temperature (20° C) relative in aquifer temperature (10° C), but even accounting for a typical factor of two enhancement of rates with a 10 degree shift in temperature (Q_{10} = 2) lab rates were still an order of magnitude greater. Instead, much of the enhancement was likely due to some degree of carbon mobilization from particles, not uncommon to slurry incubations (Smith et al. 2012). These observed rates, on the order of 1-88 nM-N/g/day for anammox and 19-1800 nM-N/g/ day for denitrification, are nevertheless slow relative to analogous rates for processes in coastal and estuarine sediments (Dale et al. 2009), aquatic sediments (Dalsgaard et al. 2012), ice (Rysgaard and Glud 2004) and continental shelf sediments (Dalsgaard et al 2005).

The faster overall total N_2 production observed at the upper plume relative to the lower plume was coincident with a higher observed denitrification at F575 (Smith et al. 2013). This faster rate, which was only moderately enhanced by the addition of acetate, was presumably enabled by a higher labile carbon abundance in the younger portion of the plume (Smith et al. 2012) In the lower plume, rates of anammox (28% of denitrification under no acetate conditions) were faster than the range predicted from ammonium transport model constraints that have been used to model $^{15}NH_4^+$ additions to the plume at this site (Böhlke et al. 2006). Anammox in lower plume sediments were within the range (13-1390 nmol/L/hr) of the few rates of anammox measured in groundwater, both lab rate (Moore et al. 2011) and *in situ* (Robertson et al. 2012). The ratio of anammox to denitrification up to 28% in the lower plume (Figure 11) was above the median ratio reported for most surface water sedimentary systems and soils, in which anammox rates are typically less than 10% of total N_2 loss (Dalsgaard et al. 2005; Song

and Tobias 2011). The lack of labile carbon at the downgradient site may create conditions favoring anammox, as evidenced by the higher anammox to denitrification ratio seen.

ORGANIC CARBON INDUCED SHIFT TO DENITRIFICATION

The addition of acetate to incubation treatments was designed to permit comparison of isotope dynamics under conditions where anammox and denitrification approximated the ratio observed in the aquifer (nonacetate), in contrast to conditions that were heavily dominated by denitrification (+ acetate). Although anammox bacteria can reportedly use some carbon substrates, including acetate, (Nicholls and Trimmer 2009; Russ et al. 2012) the stimulation of anammox rates by acetate is insubstantial relative to the well-documented enhancement of denitrification by this carbon source (Dalsgaard et al. 2005; Ginige et al. 2005; Seitzinger et al. 2006).

Nonacetate treatments always proceeded at a slower rate than those of acetate treatments regardless of plume location. Increased electron supply allowed faster reaction rates with an enhanced effect on rates of NO_x reduction and N_2 production. (Figs 3-7). The greatest effect on rates of DIN drawdown and conversion to N_2 was seen in the lower plume sediments. Differences between treatments were particularly pronounced in the downgradient 2013 experiment, for which the nonacetate treatment exhibited only a small amount of N conversion to N_2 even after 93 days of incubation. With a large NH_4^+ and NO_3^- background at this site, along with being in the core of the plume, this slow reaction rate may explain the persistence of the DIN load in the plume.

Denitrification is believed to terminate at N_2O in electron-limited environments (Seitzinger et al. 2006). While denitrification was occurring in all incubations, those that

included acetate showed less accumulation of N_2O relative those without acetate, indicating that the added carbon provided additional reducing power to push denitrification past N_2O in these low carbon sediments (Figure 3-7). The effect of acetate on the timing and accumulation of N_2O was most pronounced in the lower plume (F168) (Figure 5.a) which contains older and lower amounts of organic carbon groundwater and where *in situ* expression of the nitrous oxide reductase (*nosZ*) gene was very low (Song per. Com.). Direct validation of this acetate-induced denitrification was confirmed by the addition of ^{15}N tracer to the F168 sediments which induced a shift from a denitrification : anammox (D:A) ratio of 72% in the absence of acetate (treatment "#MI") to a D:A ratio of > 92% when acetate was added (treatment "CMI") (Fig 11-12). This nonacetate ratio of D:A for F168 in the incubations was larger than the D:A measured *in situ* following a $^{15}NO_2^-$ injection (D:A = 70:30), and may again indicate some degree of carbon mobilization from particles and enhanced carbon availability relative to *in situ* conditions (Smith et al. 2012). The smaller effect of acetate addition on the DIN dynamics in the upper plume (at all depths) where carbon is more abundant and labile (Smith et al. 2012) and D:A already high at 90% (Böhlke per. Com.) is further evidence that the acetate acted to increase denitrification relative to anammox, particularly in the lower plume. Collectively, these lines of evidence suggest that isotope enrichment factors and isotope dynamics in lower plume sediments should reflect a mixture of anammox and denitrification on the order of 1:3 in the nonacetate incubations, but almost exclusively denitrification in the acetate treatment. The isotope dynamics in the upper plume incubations should reflect the overwhelming influence of denitrification regardless of acetate treatment.

NO_x ISOTOPES AS A DIAGNOSTIC OF ANAMMOX

<u>*NOx -*</u> The observed, or apparent, enrichment factors estimated from the Rayleigh plots (Figure 7-8) represent a composite of the fractional contributions and isotopic fractionations of all reactions that interact with the specific nitrogen species measured. Poor Rayleigh fits typically indicate several competing reactions either supplying or consuming a particular species and consisting of different enrichment factors. Good Rayleigh fits typically indicate either a dominance of one reaction affecting the concentration and isotopic composition of the pool, or, if there are multiple reactions – similar enrichment factors among them. The NO_2^- and NO_3^- Rayleigh plots (Figure 8-9, Table 2) showed good linear fits at both plume locations and under both acetate and nonacetate treatments. Only the F168 lower plume nonacetate treatments (#MI) yielded unique enrichment factors for NO_3^- reduction to NO_2^-, and these two values were widely different. At -8 and -35‰, they are just outside of the range of isotope effects reported for denitrification (-13-30‰; Barford et al. 1999; Delwiche and Steyn 1970; and Granger et al. 2008) in pure culture, and in other groundwater denitrification experiments; Mariotti et al. 1981 (-24.6‰ - -29.8‰), Aravena and Robert 1998 (-22.9‰) measured under similar experimental conditions. The highly variable apparent isotope effect for NO_3^- reduction measured in this study may indicate some isotopic disequilibrium between NO_3^- and NO_2^-, particularly when reaction rates are low (F168 2013 #MI; Brunner et al. 2013). The apparent NO_2^- reduction isotope effects measured in this study were within the greater third of enrichment factors reported for denitrification (-5-25‰; Mariotti et al. 1981; Bryan et al. 1983, epsilon Casciotti 2002). With the exception of the upper plume deep sediments (#MI) which yielded an isotope effect/enrichment factor equivalent to that reported for NO_2^- reduction by a single anammox

culture (-16‰), all other measured NO_2^- reduction enrichment factors were 3–10‰ larger than what would be expected currently from anammox (Brunner et al. 2013).

The smaller NO_2^- reduction enrichment factors in the upper plume sediments versus lower plume sediments in the absence of acetate suggested a potential difference in the partitioning of different NO_2^- reduction pathways (e.g. anammox and denitrification). However, the smaller enrichment factor was found in the upper plume, where there was a larger *in situ* D:A (Smith et al. 2012). Given a NO_2^- reduction enrichment factor for anammox of -16‰; (Brunner et al. 2013), but a wider range of greater isotope effects for denitrification, a higher magnitude enrichment factor would have been expected at the larger D:A at the upper plume. Further, the addition of acetate, which forced both upper and lower plume incubations towards denitrification, did not yield significant shifts in the apparent isotope effects on NO_2^- reduction relative to no acetate conditions in either sediment type. An explanation other than differential contributions of anammox and denitrification, must be responsible for the difference in apparent isotope effects in the upper and lower plumes in the absence of added carbon. Given the magnitudes of measured enrichment factors, the range of published values, and the lack of a clear shift in enrichment factors in the presence/absence of acetate, the NO_2^- isotopes are not clearly diagnostic of a shift from anammox + denitrification to denitrification at either site.

AMMONIUM ISOTOPES AS A DIAGNOSTIC

Ammonium - The Rayleigh model could not be used to estimate effective enrichment factors for changing NH_4^+ in any of the incubations. The very poor fits (Fig 11) to all of the NH_4^+ and $\delta^{15}NH_4^+$ data were initially thought to be attributable to two distinct phases of NH_4^+ processing: an initial aerobic ammonium oxidation phase when trace O_2 was present, and a

subsequent anaerobic NH_4^+ processing phase which would include anammox. All experiments showed initial small amount of NH_4^+ consumption, likely due to aerobic ammonium oxidation fueled by the trace O_2 entrained during incubation set up. Many of the incubations (Figure 4-6) showed concurrent transient rises in NO_2^- and/or NO_3^- during this period, and the pattern of $\delta^{15}NO_2^-$/ NO_3^- at this time were consistent with aerobic ammonium oxidation. Upgradient, this initial NH_4^+ drawdown was followed by little change in NH_4^+ concentration. Downgradient with ambient NH_4^+ present, the drawdown was followed by a large fluctuation within a range of 100 μM. To deconstruct the effect of ammonium oxidation, we parsed the NH_4^+ data for each incubation into periods of >10 μM O_2 (where aerobic ammonium oxidation may dominate) and <10 μM O_2 (where the concentration and isotope effects of the oxidation would be inhibited). The differentiation showed the initial NH_4^+ concentration decrease and enrichment of $\delta^{15}NH_4^+$ (Figure 3-7) associated with the presence of trace oxygen. The separation only improved the fit of the Rayleigh curve sufficiently in two treatments to yield an enrichment factor estimate. This estimate, for the trace O_2 period, likely reflects aerobic ammonium oxidation though the fitted enrichment factors are small relative to those published for $NH_4^+ \rightarrow NO_2^-$. This apparent dampening of the isotope effect is probably due to isotopic exchange of NH_4^+ between the aqueous and sediment fractions. With a large and exchangeable ammonium pool, low rates of any fractionating reaction (aerobic ammonium oxidation, anammox, etc.) would yield only small detectable isotopic changes in the sampled aqueous NH_4^+ fraction. Detection of this potentially small signal could be hampered by small fractionations associated with sorption/desorption reactions between the NH_4^+ (aqueous) and the NH_4^+ (sediment) (Böhlke et al. 2006). Any lags in reestablishing equilibrium between the isotopically light added NH_4^+ (4‰), the isotopically heavy *in situ* NH_4^+ (15‰) and fractionation reactions would be manifested as variability in the

measured aqueous $\delta^{15}NH_4^+$. It is possible that this factor is amplified in a laboratory setting relative to *in situ* where the timescale of sampling is short in comparison to groundwater transit times. This explanation could reconcile why a robust Rayleigh defined ammonium isotope effect for anammox is measurable in sediment free cultures (Brunner et al. 2013), and inferred on large spatial and temporal scales in aquifers (Clark et al. 2008), but not in our experimental set-up. A second possible explanation that DNRA contributed to poor $NH_4^+/\delta^{15}NH_4^+$ Rayleigh fits seems unlikely given that the results of the ^{15}N tracer experiments showed DNRA was never more than 4% of the total NO_2^- reduction.

ISOTOPE MODELING

The finite difference time-stepping isotope model was constructed with experimental tracer-derived rates and other reported enrichment factors as constraints on N reactions and ratios. It was designed to specifically illuminate three aspects of the results. First, to determine the enrichment factors for respective N reactions in the natural abundance incubations that represented a "best fit" for concentrations and $\delta^{15}N$ evolution of NO_2^-, NO_3^-, NH_4^+, N_2 concentration and N_2O concentration. These reactions included: nitrate reduction ($NO_3^- \rightarrow NO_2^-$), denitrification ($NO_2^- \rightarrow N_2O$; $N_2O \rightarrow N_2$), anammox ($NO_2^- \rightarrow N_2$; $NH_4^+ \rightarrow N2$; $NO_2^- \rightarrow NO_3^-$), aerobic ammonium oxidation ($NH_4^+ \rightarrow NO_2^-$), nitrification ($NO_2^- \rightarrow NO_3^-$) (also a side reaction of anammox), and dissimilatory nitrate/nitrite reduction to ammonium ($NO_2^- \rightarrow NH_4^+$). Second, to determine whether or not the weighting of denitrification in the acetate treatments necessitated significant changes in the enrichment factors in order to maintain good model fit. Third, to determine if the observed isotope dynamic could be achieved with reasonable

enrichment factors in the complete absence of anammox. This last task addressed directly whether a portion of the isotope dynamic was clearly indicative of anammox.

The model was initialized first using a range of enrichment factors as reported in Mariotti et al. 1981, Bartford et al. 1999, Casciotti 2002, Casciotti et al. 2003; Granger et al. 2008, and Casciotti 2009. Enrichment factors and rates are adjusted to yield optimum fits while remaining constrained by the range in the literature. The DNRA, denitrification, and anammox rates relative to each other were constrained by results from the tracer incubations. The range of acceptable D:A ratios was 0-0.50; the range of DNRA as a percentage of NO_2^- reduction was 0-4%.

Model fits under "natural" (no acetate) conditions yielded similar parameters for both upgradient and downgradient sites. When parameters were set to achieve best model fits, enrichment factors ranged from -18-25‰ for all reactions. For the denitrification steps, including nitrate reduction ($NO_3^- \rightarrow NO_2^- \rightarrow N_2O \rightarrow N_2$), enrichment factors were -20, -18, and -22‰. All of these values were within reported ranges, with the exception of $N_2O \rightarrow N_2$ which was approximately 10‰ greater (Barford et al. 1999; Ostrom et al. 2007). For anammox, $NO_2^- \rightarrow N_2$ had an enrichment factor of -25‰, and $NH_4^+ \rightarrow N_2$ generated an enrichment factor of -23‰. DNRA and aerobic ammonium oxidation were also found with enrichment factors of -20‰. Optimum A:D was 0.08, with the DNRA ratio to NO_2^- reduction at 0.02. At the downgradient site, isotope effects ranged from -16-30‰. Denitrification steps had enrichment factors of -25, -25, and -30‰. For anammox, the $NO_2^- \rightarrow N_2$ reaction had an enrichment factor of -16‰, and the $NH_4^+ \rightarrow N_2$ reaction had an enrichment factor of -23‰. DNRA was inactive for this model. Aerobic ammonium oxidation was at -20‰. A:D ratio was set at 0.18. All these enrichment factors in the nonacetate treatments were in range of those required for denitrification

(Barford et al. 1999; Granger et al. 2008; Bryan et al. 1983; Casciotti et al. 2002; Mariotti et al. 1981). With the exception of $N_2O \rightarrow N_2$, whose modeled ε was ~10‰ greater than previously reported (Barford et al. 1999; Ostrom et al. 2007), all modeled isotope effects for denitrification in the upper and lower plume were within reported ranges (Barford et al.1999; Granger et al. 2006; Casciotti et al. 2002). It was difficult to achieve good fits to the $\delta^{15}N_2$ data without the large $N_2O \rightarrow N_2$ enrichment factors, indicating that this higher fractionation in the final denitrification step is characteristic of the system. The isotope effects for anammox reactions ($NO_2^- \rightarrow N_2$ and $NH_4^+ \rightarrow N_2$) were largely consistent with the one published summary of anammox enrichment factors (Brunner et al. 2013). One greater modeled enrichment factor for $NO_2^- \rightarrow N_2$ in the upper plume (-25‰ versus a published -16‰) was relatively unimportant in the overall model. The model was sensitive to changes in denitrification parameters, but due to the low A:D ratio even in lower plume, changes in anammox reaction enrichment factors only moderately influenced overall model fit.

F575 #MI

Anammox : Denit	fDNRA
0.08	0.02

Pathway	Reaction	Redox lag k	Vmax	Ks	α	-ε
$NO_3^- \rightarrow NO_2^-$	Nitrate Reduction	1	0.030	5	0.980	20
$NO_2^- \rightarrow N_2O$	Denitrification I	0.09	0.130	1	0.982	18
$NO_2^- \rightarrow N_2^*$	Anammox	0.05	0.004	5	0.975	25
$NO_2^- \rightarrow NO_3^-$	Anammox	0.05	0.004	5	1.030	-30
$NO_2^- \rightarrow NH_4^+$	DNRA	0.05	0.004	1	0.980	20
$NO_2^- \rightarrow NO_3^-$	Nitrification	10	0.030	5	1.012	-12
$NH_4^+ \rightarrow NO_2^-$	Aerobic Am Oxidation	10	0.001	5	0.980	20
$^*NH_4^+ \rightarrow N_2$	*Anammox	0.05	0.004	5	0.977	23
$N_2O \rightarrow N_2$	Denit II	0.02	0.38	1	0.978	22

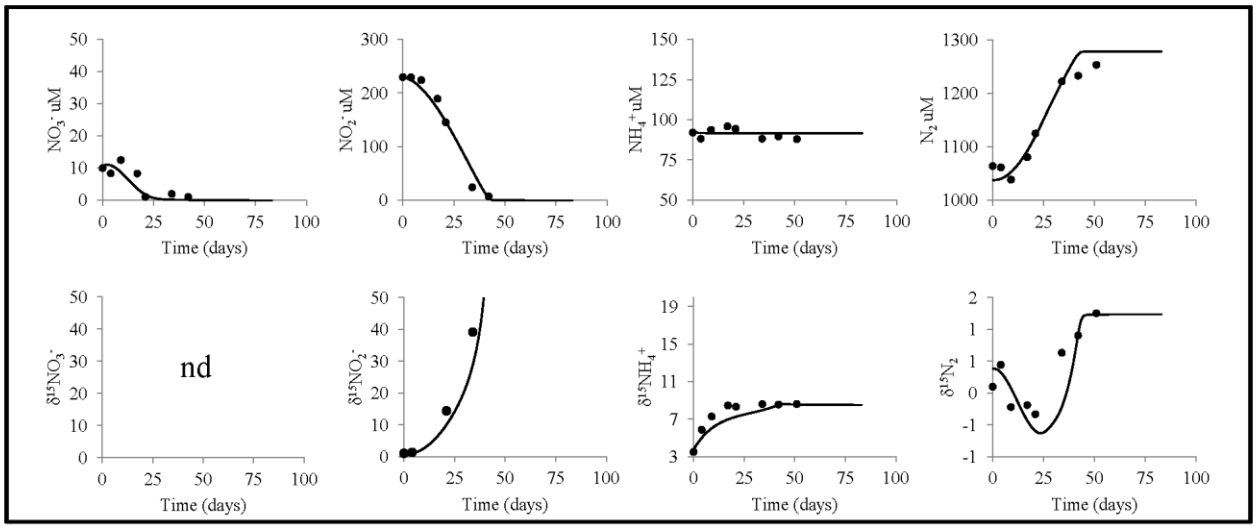

Figure 11. Best model fits to data from the 2012 upgradient nonacetate treatment. The anammox:denitrification ratio is located above the table, next to the rate of DNRA occurring proportional to them. In the table, the pathway is to the far left, with its reaction name beside it. Fractionation factors (α) are shown beside their corresponding enrichment factors (ε). In the plots, the points indicate experimental data from the treatment, and the smoothed line is generated from the model for a best fit.

F168 #MI

Anammox : Denit	fDNRA
0.18	0.00

Pathway	Reaction	Redox lag k	Vmax	Ks	α	-ε
$NO_3^- \rightarrow NO_2^-$	Nitrate Reduction	0.5	0.070	5	0.975	25
$NO_2^- \rightarrow N_2O$	Denitrification I	0.3	0.110	5	0.975	25
$NO_2^- \rightarrow N_2^-$	Anammox	0.08	0.012	5	0.984	16
$NO_2^- \rightarrow NO_3^-$	Anammox	0.08	0.012	5	1.030	-30
$NO_2^- \rightarrow NH_4^+$	DNRA	0.08	0.000	5	0.975	25
$NO_2^- \rightarrow NO_3^-$	Nitrification	10	0.050	5	1.010	-10
$NH_4^+ \rightarrow NO_2^-$	Aerobic Am Oxidation	10	0.070	5	0.980	20
$^*NH_4^+ \rightarrow N_2$	*Anammox	0.08	0.012	5	0.977	23
$N_2O \rightarrow N_2$	Denit II	0.05	1	5	0.970	30

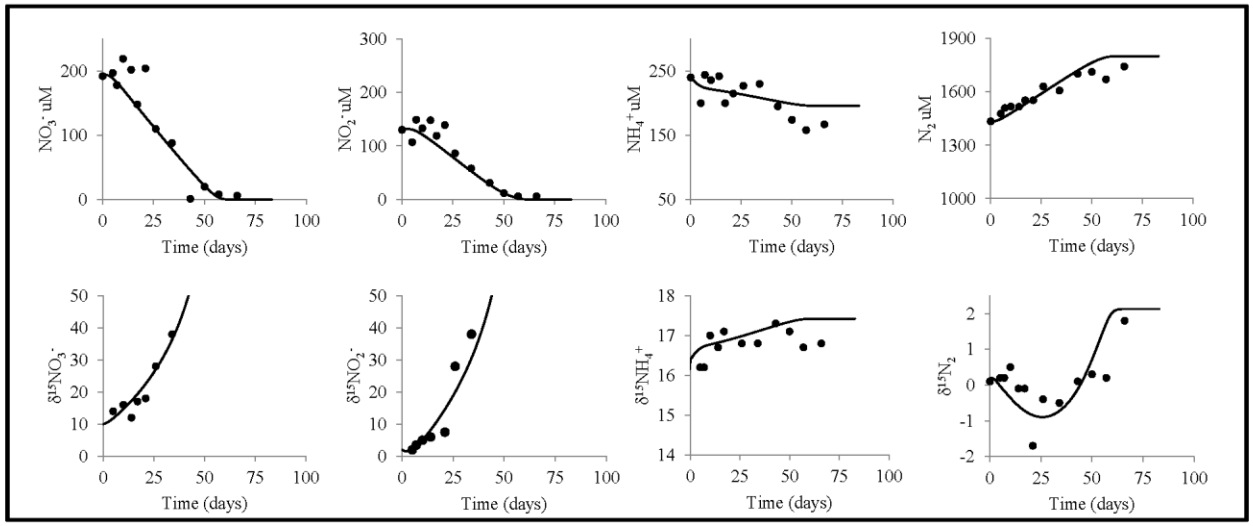

Figure 12. Best model fits to data from the 2012 downgradient nonacetate treatment. The anammox:denitrification ratio is located above the table, next to the rate of DNRA occurring proportional to them. In the table, the pathway is to the far left, with its reaction name beside it. Fractionation factors (α) are shown beside their corresponding enrichment factors (ε). In the plots, the points indicate experimental data from the treatment, and the smoothed line is generated from the model for a best fit.

When acetate was added to shift the N_2 production to denitrification (minimizing anammox), similar fits could be achieved by adjusting denitrification rates and enrichment factors within a reasonable range for both upgradient and downgradient (Figures 13 and 14). NO_2^- concentration and isotopes continued to be dominated by denitrification. The fits for NO_3^- and $^{15}NO_3^-$ were unaffected by presence or absence of the $NO_2^- \rightarrow NO_3^-$ reaction component of anammox. The influence of anammox on the NH_4^+ isotopes was similarly negligible. The NH_4^+ isotopes were largely governed by aerobic ammonium oxidation at the beginning of incubations, and isotope exchanges between aqueous and sediment ammonium. Even when the #MI treatments were modeled with anammox removed, good model fits could be attained. Similarly because DNRA had a small rate, it did not play a significant role in model fitting for either NO_2^- or NH_4^+ at any site for any treatment.

F575 CMI

Anammox : Denit	fDNRA
0.07	0.00

Pathway	Reaction	Redox lag k	Vmax	Ks	α	-ε
$NO_3^- \rightarrow NO_2^-$	Nitrate Reduction	1	0.030	5	0.980	20
$NO_2^- \rightarrow N_2O$	Denitrification I	0.1	0.180	5	0.982	18
$NO_2^- \rightarrow N_2^-$	Anammox	0.5	0.006	5	0.975	25
$NO_2^- \rightarrow NO_3^-$	Anammox	0.5	0.006	5	1.020	-20
$NO_2^- \rightarrow NH_4^+$	DNRA	0.5	0.000	5	0.990	10
$NO_2^- \rightarrow NO_3^-$	Nitrification	10	0.030	5	1.010	-10
$NH_4^+ \rightarrow NO_2^-$	Aerobic Am Oxidation	10	0.010	5	0.995	5
$^*NH_4^+ \rightarrow N_2$	*Anammox	0.5	0.006	5	0.977	23
$N_2O \rightarrow N_2$	Denit II	0.1	0.17	1	0.98	20

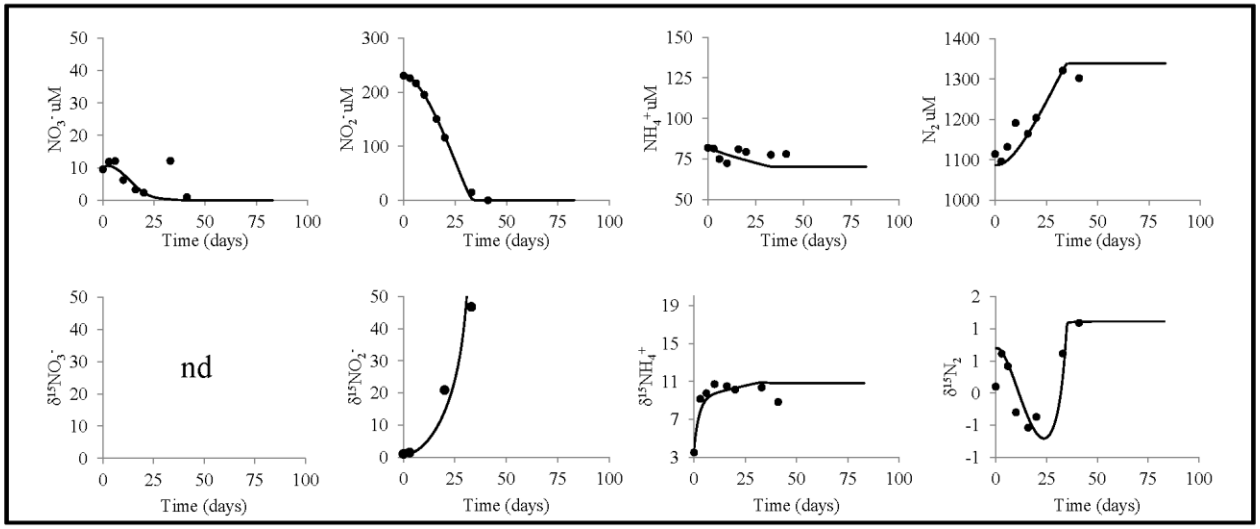

Figure 13. Best model fits to data from the 2012 upgradient acetate treatment. The anammox:denitrification ratio is located above the table, next to the rate of DNRA occurring proportional to them. In the table, the pathway is to the far left, with its reaction name beside it. Fractionation factors (α) are shown beside their corresponding enrichment factors (ε). In the plots, the points indicate experimental data from the treatment, and the smoothed line is generated from the model for a best fit.

F168 CMI

Anammox : Denit	fDNRA
0.02	0.00

Pathway	Reaction	Redox lag k	Vmax	Ks	α	-ε
$NO_3^- \rightarrow NO_2^-$	Nitrate Reduction	1	0.150	5	0.980	20
$NO_2^- \rightarrow N_2O$	Denitrification I	0.5	0.180	5	0.980	20
$NO_2^- \rightarrow N_2^-$	Anammox	0.5	0.002	5	0.984	16
$NO_2^- \rightarrow NO_3^-$	Anammox	0.5	0.002	5	1.030	-30
$NO_2^- \rightarrow NH_4^+$	DNRA	0.5	0.000	5	0.975	25
$NO_2^- \rightarrow NO_3^-$	Nitrification	10	0.160	5	1.010	10
$NH_4^+ \rightarrow NO_2^-$	Aerobic Am Oxidation	10	0.150	5	0.980	20
$^*NH_4^+ \rightarrow N_2$	*Anammox	0.5	0.002	5	0.977	23
$N_2O \rightarrow N_2$	Denit II	0.1	0.45	5	0.977	23

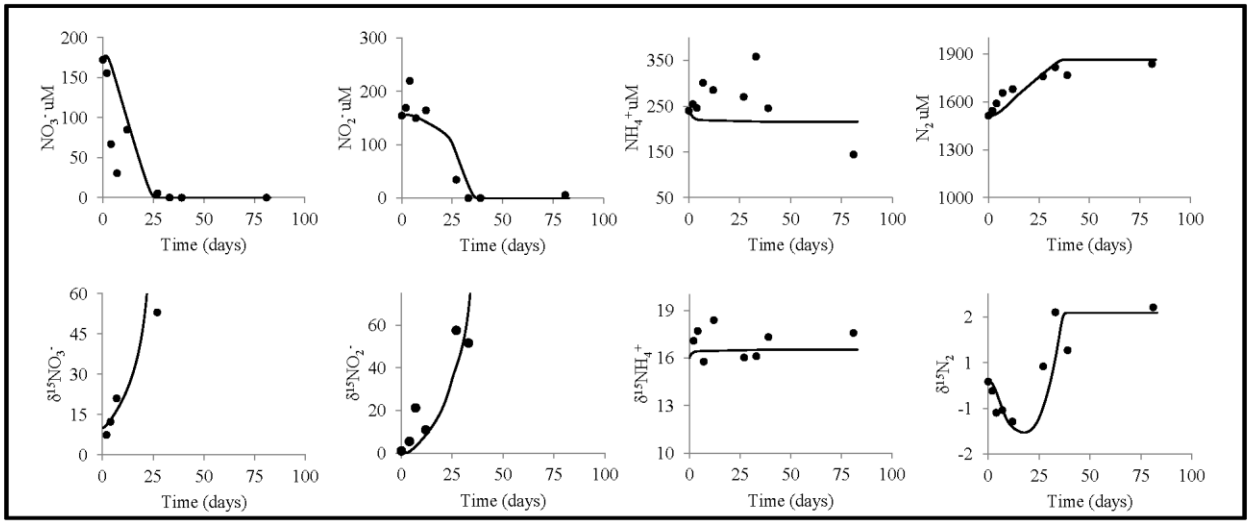

Figure 14. Best model fits to data from the 2012 downgradient acetate treatment. The anammox:denitrification ratio is located above the table, next to the rate of DNRA occurring proportional to them. In the table, the pathway is to the far left, with its reaction name beside it. Fractionation factors (α) are shown beside their corresponding enrichment factors (ε). In the plots, the points indicate experimental data from the treatment, and the smoothed line is generated from the model for a best fit.

SUMMARY

While a signal for anammox can be detected and confirmed through tracer experiments, we were unable to establish a clear isotopic diagnostic for any DIN species that would be indicative of anammox under conditions where denitrification co-occurs. In the Cape Cod plume, there was a sufficient fractionation overlap between denitrification and anammox reactions involving shared oxidized N pools to preclude distinction between $^{15}NO_x$ isotopes. Use of the $\delta^{15}NH_4^+$ pool was hampered by a combination of low rates of NH_4^+ use by anammox and variable amounts of NH_4^+ isotope exchanges between aqueous and sediment fractions. It is possible that the dampening of the anammox isotope effect caused by these exchanges may diminish on plume transport scales. On these extended time scales, low anammox rates could remove enough total NH_4^+ enough to potentially detect an anammox fractionation in the NH_4^+ pool (Clark et al. 2008). However, the chromatographic and isotope homogenization effect of these isotope exchanges should be carefully considered when using *in situ* patterns of $\delta^{15}NH_4^+$ to infer anammox.

REFERENCES

An, S, and Joye, SB. 2001. Enhancement of coupled nitrification-denitrification by benthic photosynthesis in shallow estuarine sediments. *Limnol. Oceanography*. **46 (1)**: 62-74.

Appelo, CAJ, and Postma, D. 2005. Geochemistry, Groundwater and Pollution. 2nd edition. *A.A. Balkema Publishers, Leiden, The Netherlands*.

Aravena, R, and Robertson, WD. 1998. Use of multiple isotope tracers to evaluate denitrification in ground water: Study of nitrate from a large-flux septic system plume. *Ground Water*. **36**: 975–982.

Armstrong, FAJ, et al. 1967. The measurement of upwelling and subsequent biological processes by means of the Technicon_ AutoAnalyzer_ and associated equipment. *Deep-Sea Res.* **14 (3)**: 381-389.

Barbaro, JR, et al. 2013. Transport of Nitrogen in a Treated-Wastewater Plume to Coastal Discharge Areas, Ashumet Valley, Cape Cod, Massachusetts. *U.S. Geological Survey Toxic Substances Hydrology Program: Scientific Investigations Report 2013-5061*.

Bartford, CC, et al. 1999. Steady-state Nitrogen isotope effects of N_2 and N_2O production in *Paracoccus denitrificans*. *Applied Environmental Microbiology*. **65:** 989-994

Böhlke, JK, and Denver, JM. 1995. Combined Use of Groundwater Dating, Chemical, and Isotopic Analyses to Resolve the History and Fate of Nitrate Contamination in Two Agricultural Watersheds, Atlantic Coastal Plain, Maryland. *Water Resources Research*. **31 (9)**: 2319-2339

Böhlke, JK. 2001. Groundwater recharge and agricultural contamination. *Hydrogeology Journal*. **10:** 153-179.

Böhlke, JK, et al. 2002. Denitrification in the recharge area and discharge area of a transient agricultural nitrate plume in a glacial outwash sand aquifer, Minnesota. *Water Resources Research*. **38 (7): 10**-1-26

Böhlke, JK, et al. 2004. Reach-scale isotope tracer experiment to quantify denitrification and related processes in a nitrate-rich stream, midcontinent United States. *Limnol. Oceanography*. **49 (3)**: 821-838

Böhlke, JK, et al. 2006. Ammonium transport and reaction in contaminated groundwater: Application of isotope tracers and isotope fractionation studies. *Water Resources Research*. **42**: 1-19

Böhlke, JK, et al. 2009. Multi-scale measurements and modeling of denitrification in streams with varying flow and nitrate concentration in the upper Mississippi River basin, USA. *Biogeochemistry*. **93**: 117-141

Bouwman, AF, et al. 1995. Uncertainties in the global source distribution of nitrous oxide. *Journal of Geophysical Research: Atmospheres*. **100 (D2)**: 2785-2800

Bouwman, AF, et al. 2002. Modeling global annual N_2O and NO emissions from fertilized fields. *Global Biogeochemical Cycles*. **16 (4)**: 28-1 – 28-9

Brunner, B, et al. 2013. Nitrogen isotope effects induced by anammox bacteria. *PNAS*. **110 (47)**: 18994-18999

Bryan, BA, et al. 1983. Variable expression of the nitrogen isotope effect associated with denitrification of nitrite. *Journal of Biological Chemistry*. **258**: 8613-8617

Burgin, AJ, et al. 2010. Factors Regulating Denitrification in a Riparian Wetland. *Soil Science Society of America Journal*. **74 (5)**: 1826-1833

Casciotti, KL, et al. 2002. Measurement of the oxygen isotopic composition of nitrate in seawater and freshwater using the denitrifier method. *Analytical Chemistry*. **74 (19)**: 4905-4912

Casciotti, KL, et al. 2003. Linking diversity and stable isotope fractionation in ammonia-oxidizing bacteria. *Geomicrobiol. J.* **20**: 335-353

Casciotti, KL. 2009. Inverse kinetic isotope fractionation during bacterial nitrite oxidation. *Geochimica et Cosmochimica Acta*. **73 (7)**: 2061-2076

Clark, I, et al. 2008. Origin and Fate of Industrial Ammonium in Anoxic Ground Water – ^{15}N Evidence for Anaerobic Oxidation (Anammox). *Ground Water Monitoring & Remediation*. **28 (3)**: 73-82

Cole, ML, et al. 2006. Effects of watershed land use on nitrogen concentrations and d15 nitrogen in groundwater. *Biogeochemistry*. **77**: 199-215

Dale, OR, et al. 2009. Biogeographical distribution of diverse anaerobic ammonium oxidizing (anammox) bacteria in Cape Fear River Estuary. *Environmental Microbiology*. **11 (5)**: 1194-1207

Dalsgaard, T, et al. 2003. N_2 production by the anammox reaction in the anoxic water column of Golfo Dulce, Costa Rica. *Nature*. **422:** 606-608

Dalsgaard, T, et al. 2005. Anaerobic ammonium oxidation (anammox) in the marine environment. *Research in Microbiology*. **156**: 457-464

Dalsgaard, T, et al. 2012. Anammox and denitrification in the oxygen minimum zone of the eastern South Pacific. *Limnol. Oceanography*. **57 (5)**: 1331-1346

Deegan, LA, et al. 2002. Nitrogen loading alters seagrass ecosystem structure and support of higher trophic levels. *Aquatic Conservation: Marine and Freshwater Ecosystems.* **12 (2)**: 193-212

Delwich, CC, and Steyn, PL. 1970. Nitrogen isotope fractionation in soils and microbial reactions. *Environmental Science and Technology*. **4:** 929-935

Galloway, JN, et al. 2003. The Nitrogen Cascade. *BioScience*. **53 (4)**: 341-356

Garabedian SP, et al. 1991. Large-scale natural gradient tracer test in sand and gravel, Cape Cod, Massachusetts: 2. Analysis of spatial moments for a nonreactive tracer. *Water Resources Research*. **27 (5)**: 911-924

Giblin, AE, and Gaines, AG. 1990. Nitrogen inputs to a marine embayment: the importance of groundwater. *Biogeochemistry*. **10**: 309-328

Giblin, AE, et al. 2013. The importance of dissimilatory nitrate reduction to ammonium (DNRA) in the nitrogen cycle of coastal ecosystems. *Oceanography*. **26 (3)**: 124-131

Ginige, MP, et al. 2005. Investigation of an Acetate-Fed Denitrifying Microbial Community by Stable Isotope Probing, Full-Cycle rRNA Analysis, and Fluorescent In Situ Hybridization-Microautoradiography. *Applied Environmental Microbiology.* **71 (12)**: 8683-8691

Granger, J, et al. 2006. A method for nitrite removal in nitrate N and O isotope analyses. *Limnol. Oceanographic Methods*. **4**: 205-212

Granger, J, et al. 2008. Nitrogen and oxygen isotope fractionation during dissimilatory nitrate reduction by denitrifying bacteria. *Limnol. Oceanography.* **56 (6)**: 2533-2545

Green, CT, et al. 2010. Mixing effects on apparent reaction rates and isotope fractionation during denitrification in a heterogeneous aquifer. *Water Resources Research.* **46 (8)**: W08525

Hamersley, RM, et al. 2009. Water column anammox and denitrification in a temperate permanently stratified lake (Lake Rassnitzer, Germany). *Systematic and Applied Microbiology*. **32 (8)**: 571-582

Harrison, MD, et al. 2011. Denitrification in Alluvial Wetlands in an Urban Landscape. *Journal of Environmental Quality*. **40 (2)**: 634-646

Hillebrand, H, et al. 2000. Marine microbenthic community structure regulated by nitrogen loading and grazing pressure. *Marine Ecology Progress Series*. **204:** 27-38

Holmes, RM, et al. 1999. A simple and precise method for measuring ammonium in marine and freshwater ecosystems. *Canadian Journal of Fisheries and Aquatic Sciences*. **56 (10)**: 1801-1808

Howarth, RW, and Marino, R. 2006. Nitrogen as the limiting nutrient for eutrophication in coastal marine ecosystems: Evolving views over three decades. *Limnol. Oceanography*. **51 (1, part 2)**: 364-376

Huang, J, et al. 2008. Estimation of regional emissions of nitrous oxide from 1997 to 2005 using multinetwork measurements, a chemical transport model, and an inverse method. *Journal of Geophysical Research: Atmospheres*. **113 (D17)**: 16

Hyun, S, et al. 2013. Variability in Nitrate and Ammonium Distributions and Associated Processes at the Groundwater/Surface-water Interface in a Groundwater Flow-through Pond. *American Geophysical Union, Fall Meeting 2013*. Abstract #H33F-1441

Jahangir, MMR, et al. 2013. Quantification of In Situ Denitrification Rates in Groundwater Below an Arable and a Grassland System. *Water Air Soil Pollut.* **224**: 1693

Jetten, MS, et al. 2001. Microbiology and application of the anaerobic ammonium oxidation ('anammox') process. *Current Opinion in Biotechnology*. **12**: 283-288

Kartal, B, et al. 2007. Anammox bacteria disguised as denitrifiers: nitrate reduction to dinitrogen gas via nitrite and ammonium. *Environmental Microbiology*. **9 (3):** 635-642

Kartal, B, et al. 2008. *Candidatus* 'Brocadia fulgida': an autofluorescent anaerobic ammonium oxidizing bacterium. *FEMS Microbiology Ecology*. **63 (1)**: 46-55

Kalvelage, T, et al. 2011. Oxygen Sensitivity of Anammox and Coupled N-Cycle Processes in Oxygen Minimum Zones. *PLoS ONE*. **6 (12)**: e29299

Körner, H, and Zumft, WG. 1989. Expression of Denitrification Enzymes in Response to the Dissolved Oxygen Level and Respiratory Substrate in Continuous Culture of *Pseudomonas stutzeri*. *Applied and Environmental Microbiology*. **55 (7)**: 1670-1676

Kritee, K, et al. 2012. Reduced isotope fractionation by denitrification under conditions relevant to the ocean. *Geochimica et Cosmochimica Acta*. **92 (1)**: 243-259

Kuypers, MMM, et al. 2003. Anaerobic ammonium oxidation by anammox bacteria in the Black Sea. *Nature*. **422**: 608-610

Lam, P, et al. 2007. Linking crenarchaeal and bacterial nitrification to anammox in the Black Sea. *PNAS*. **104 (17)**: 7104-7109

Lam, P, et al. 2009. Revising the nitrogen cycle in the Peruvian oxygen minimum zone. *PNAS*. **106 (12)**: 4752-4757

Lyngkilde, J, and Christensen, TH. 1992. Redox zones of a landfill leachate pollution plume (Vejen, Denmark). *Journal of Contaminant Hydrology*. **10**: 273-289

Nicholls, JC, and Trimmer, M. 2009. Widespread occurrence of the anammox reaction in estuarine sediments. *Aquatic Microbial Ecology.* **55:** 105-113

Mariotti, A, et al. 1981. Experimental Determination of Nitrogen Kinetic Isotope Fractionation: Some Principles; Illustration for the Denitrification and Nitrification Processes. *Plant and Soil*. **62**: 413-430

Mariotti, A, et al. 1982. Nitrogen isotope fractionation associated to the NO2- → N2O step of denitrification in soils. *Canadian Journal of Soil Science*. **62 (2)**: 227-241

Mariotti, A, et al. 1988. 15N isotope biogeochemistry and natural denitrification process in groundwater: Application to the chalk aquifer of northern France. *Geochimica et Cosmochimica Acta*. **52**: 1869-1878

Moore, TA, et al. 2011. Prevalence of Anaerobic Ammonium-Oxidizing Bacteria in Contaminated Groundwater. *Environmental Science and Technology.* **45**: 7217-7225

Mulder, A, et al. 1995. Anaerobic ammonium oxidation discovered in a denitrifying fluidized bed reactor. *FEMS Microbiology Ecology*. **16**: 177-184

Ostrom, NE, et al. 2007. Isotopologue effects during N_2O reduction in soils and in pure cultures of denitrifiers. *Journal of Geophysical Research*. **112:** G02005

Perez, T, et al. 2006. Nitrous Oxide Nitrification and Denitrification 15N Enrichment Factors from Amazon Forest Soils. *Ecological Applications*. **16 (6)**: 2153-2167

Paerl, HW. 1997. Coastal eutrophication and harmful algal blooms: Importance of atmospheric deposition and groundwater as "new" nitrogen and other nutrient sources. *Limnol. Oceanography.* **42 (5, part 2)**: 1154-1165

Prokopenko, MG, et al. 2013. Nitrogen losses in anoxic marine sediments driven by Thioplaca-anammox bacterial consortia. *Nature*. **500**: 194-198

Risgaard-Petersen, N. 2003. Coupled nitrification-denitrification in autotrophic and heterotrophic estuarine sediments: On the influence of benthic microalgae. *Limnol. Oceanography*. **48 (1)**: 93-105

Risgaard-Peterson, N, et al. 2003. Application of the isotope pairing technique in sediments where anammox and denitrification coexist. *Limnology and Oceanography: Methods*. **1**: 63-73

Robertson, LA, et al. 1989. Aerobic denitrification in various heterotrophic nitrifiers. *Antonie van Leeuwenhoek.* **56**: 289-299

Robertson, WD, et al. 2012. Natural Attenuation of Septic System Nitrogen by Anammox. *Groundwater*. **50 (4)**: 541-553

Russ, L, et al. 2012. Genome analysis and heterologous expression of acetate-activating enzymes in the anammox bacterium *Kuenenia stuttgartiensis*. **194 (11):** 943-948

Rysgaard, S, and Glud, RN. 2004. Anaerobic N_2 production in Arctic sea ice. *Limnol. Oceanography*. **49 (1)**: 86-94

Schalk, J, et al. 1998. The anaerobic oxidation of hydrazine: a novel reaction in microbial nitrogen metabolism. *FEMS Microbiology Letters*. **158:** 61-67

Schmid, M, et al. 2003. *Candidatus* "Scalindua brodae", sp. nov., *Candidatus* "Scalindua wagneri", sp. nov., Two New Species of Anaerobic Ammonium Oxidizing Bacteria. *Systematic and Applied Microbiology*. **26 (4)**: 529-538

Schmidt, CM, et al. 2011. Linking Denitrification and Infiltration Rates during Managed Groundwater Recharge. *Environ. Sci. Technol.* **45 (22)**: 9634-9640

Seitzinger, S, et al. 2006. Denitrification across landscapes and waterscapes: a synthesis. *Ecological Applications*. **16 (6)**: 2064-2090

Siegrist, H, et al. 1998. Nitrogen loss in a nitrifying rotating contactor treating ammonium-rich wastewater without organic carbon. *Water Science and Technology*. **38 (8-9)**: 241-248

Sliekers, AO, et al. 2002. Completely autotrophic nitrogen removal over nitrite in one single reactor. *Water Research*. **36 (10)**: 2475-2482

Smith, RL, and Duff, JH. 1988. Denitrification in a Sand and gravel Aquifer. *Applied and Environmental Microbiology.* **54 (5)**: 1071-1078

Smith, RL, et al. 1991. Denitrification in nitrate-contaminated groundwater: Occurrence in steep vertical geochemical gradients. *Geochimica et Cosmochimica Acta*. **55 (7)**: 1815-1825

Smith, RL, et al. 2001. In Situ Stimulation of Groundwater Denitrification with Formate To Remediate Nitrate Contamination. *Environmental Science and Technology*. **35 (1)**: 196-203

Smith, RL, et al. 2004. Assessment of Nitrification Potential in Ground Water Using Short Term, Single-Well Injection Experiments. *Microbial Ecology*. **51:** 22-35 (2006)

Smith, RL, et al. 2012. Long-term groundwater contamination after source removal – The role of sorbed carbon and nitrogen on the rate of reoxygenation of a treated-wastewater plume on Cape Cod, MA, USA. *Chemical Geology*. **337-338**: 38-47

Smith, RL, et al. 2013. Is Anaerobic Ammonium Oxidation ("Anammox") Important for Nitrogen Cycling in Groundwater? *Geological Society of America, 125th Anniversary Annual Meeting.* Abstract #170-7

Song, BK, et al. 2010. Molecular and Stable Isotope Investigation of Nitrite Respiring Bacterial Communities Capable of Anaerobic Ammonium Oxidation (ANAMMOX) and Denitrifying Anaerobic Methane Oxidation (DAMO) in Nitrogen Contaminated Groundwater. *American Geophysical Union, Fall Meeting 2010*. Abstract #B51B-0349

Song, BK, and Tobias, CR. 2011. Molecular and stable isotope methods to detect and measure anaerobic ammonium oxidation (anammox) in aquatic ecosystems. *Methods in Enzymology*. **496**: 63-89

Souza, VF, et al. 2012. Sediment denitrification, DNRA, and ANAMMOX rates in tropical floodplain lake (Pantanal, Brazil). *Oecologia Australis*. **16 (4)**: 734-744

Strous, M, et al. 1999. Missing lithotroph identified as new planctomycete. *Nature*. **400**: 446-449

Strous, M, et al. 2006. Deciphering the evolution and metabolism of an anammox bacterium from a community genome. *Nature*. **440**: 790-794

Sutka, RL, et al. 2008. Isotopologue fractionation during N2O production by fungal denitrification. *Rapid Communications in Mass Spectrometry*. **22 (24)**: 2989-3996

Swartz, CH, et al. 2006. Steroid Estrogens, Nonylphenol Ethoxylate Metabolites, and Other Wastewater Contaminants in Groundwater Affected by a Residential Septic System on Cape Cod, MA. *Environmental Science and Technology*. **40 (16)**: 4894-4902

Thamdrup, B, et al. 2006. Anaerobic ammonium oxidation in the oxygen-deficient waters off northern Chile. *Limnol. Oceanography*. **51**: 2145-2156

Thamdrup, B, and Dalsgaard, T. 2002. Production of N_2 through Anaerobic Ammonium Oxidation Couples to Nitrate Reduction in Marine Sediments. *Applied and Environmental Microbiology*. **63 (3)**: 1312-1318

Third, KA, et al. 2005. Treatment of nitrogen-rich wastewater using partial nitrification and anammox in the CANON process. *Water Science Technology*. **42 (4)**: 47-54

Thurman, EM, et al. 1986. Movement and fate of detergents in groundwater: a field study. *Journal of Contaminant Hydrology*. **1 (1-2)**: 143-161

Trimmer, M, et al. 2003. Anaerobic ammonium oxidation measured in sediments along the Thames estuary, United Kingdom. *Applied Environmental Microbiology*. **69:** 6447-6454

Trimmer, M, et al. 2005. Biphasic Behavior of Anammox Regulated by Nitrite and Nitrate in an Estuarine Sediment. *Applied Environmental Microbiology*. **71 (4)**: 1923-1930

Tobias, CR, et al. 2001. Tracking the fate of a high concentration groundwater nitrate plume through the fringing marsh: A combined groundwater tracer and in situ isotope enrichment study. *Limnol. Oceanography*. **46 (8)**: 1977-1989

USGS Cape Cod Toxics. 2013. Site Description and Maps. Cape Cod Toxic Substances Hydrology Research Site. [Online]. Available: http://ma.water.usgs.gov/MMRCape/sitedescription.html. [2013, May 5].

Valiela, I, et al. 1997. Macroalgal Blooms in Shallow Estuaries: Controls and Ecophysiological and Ecosystem Consequences. *Limnol. Oceanography*. **42 (5)**: 1105-1118

Valiela, I, et al. 1999. Transport of groundwater-borne nutrients from watersheds and their effects on coastal waters. *Biogeochemisty*. **10**: 177-197

Vitousek, PM, et al. 1997. Human alteration of the global nitrogen cycle: sources and consequences. *Ecol. Applications*. **7 (3)**: 737-750

Voss, M, et al. 2001. Nitrogen isotope patterns in the oxygen-deficient waters of the Eastern Tropical North Pacific Ocean. *Deep Sea Research Part I: Oceanographic Research Papers*. **48 (8)**: 1905-1921

Weatherburn, MW. 1967. Phenol-hypochlorite reaction for determination of ammonia. *Analytical Chemistry*. **39 (8):** 971-974